Discoveries

ORIGINAL RESEARCH COMMUNICATION

Oxidation of Hemoglobin Drives a Proatherogenic Polarization of Macrophages in Human Atherosclerosis

László Potor,[1–4],* Zoltán Hendrik,[1,4,5],* Andreas Patsalos,[6–9,i] Éva Katona,[10] Gábor Méhes,[5]
Szilárd Póliska,[11] Éva Csősz,[6] Gergő Kalló,[6] István Komáromi,[10] Zsolt Combi,[3,4] Niké Posta,[3,4]
Katalin Éva Sikura,[1,2] Dávid Pethő,[3,4] Melinda Oros,[3] György Vereb,[12] Csaba Tóth,[13] Péter Gergely,[14,ii]
László Nagy,[6,7,†] György Balla,[1,2,†] and József Balla[1,3,†,iii]

Abstract

Aim: The aim of our study was to explore the pathophysiologic role of oxidation of hemoglobin (Hb) to ferrylHb in human atherosclerosis.

Results: We observed a severe oxidation of Hb to ferrylHb in complicated atherosclerotic lesions of carotid arteries with oxidative changes of the globin moieties, detected previously described oxidation hotspots in Hb (β1Cys93; β1Cys112; β2Cys112) and identified a novel oxidation hotspot (α1Cys104). After producing a monoclonal anti-ferrylHb antibody, ferrylHb was revealed to be localized extracellularly and also internalized by macrophages in the human hemorrhagic complicated lesions. We demonstrated that ferrylHb is taken up *via* phagocytosis as well as CD163 receptor-mediated endocytosis and then transported to lysosomes involving actin polymerization. Internalization of ferrylHb was accompanied by upregulation of heme oxygenase-1 and H-ferritin and accumulation of iron within lysosomes as a result of heme/iron uptake. Importantly, macrophages exposed to ferrylHb in atherosclerotic plaques exhibited a proinflammatory phenotype, as reflected by elevated levels of IL-1β and TNF-α. To find further signatures of ferrylHb in complicated lesions, we performed RNA-seq analysis on biopsies from patients who underwent endarterectomies. RNA-seq analysis demonstrated that human complicated lesions had a unique transcriptomic profile different from arteries and atheromatous plaques. Pathways affected in complicated lesions included gene changes associated with phosphoinositide 3-kinase (PI3K) signaling, lipid transport, tissue

[1]ELKH-UD Vascular Biology and Myocardial Pathophysiology Research Group, Hungarian Academy of Sciences, Debrecen, Hungary.
[2]Department of Pediatrics, Faculty of Medicine, University of Debrecen, Debrecen, Hungary.
[3]Division of Nephrology, Department of Medicine, Faculty of Medicine, University of Debrecen, Debrecen, Hungary.
[4]Kálmán Laki Doctoral School, University of Debrecen, Debrecen, Hungary.
[5]Department of Pathology, Faculty of Medicine, University of Debrecen, Debrecen, Hungary.
[6]Department of Biochemistry and Molecular Biology, Faculty of Medicine, University of Debrecen, Debrecen, Hungary.
Departments of [7]Medicine and [8]Biological Chemistry, Johns Hopkins University School of Medicine, St. Petersburg, Florida, USA.
[9]Johns Hopkins All Children's Hospital, St. Petersburg, Florida, USA.
[10]Department of Laboratory Medicine, Faculty of Medicine, University of Debrecen, Debrecen, Hungary.
[11]Proteomics Core Facility, Department of Biochemistry and Molecular Biology, Faculty of Medicine, University of Debrecen, Debrecen, Hungary.
[12]Department of Biophysics and Cell Biology, Faculty of Medicine, University of Debrecen, Debrecen, Hungary.
[13]Division of Vascular Surgery, Department of Surgery, Faculty of Medicine, University of Debrecen, Debrecen, Hungary.
[14]Department of Forensic Medicine, Faculty of Medicine, University of Debrecen, Debrecen, Hungary.
*Both these authors share the first authorship.
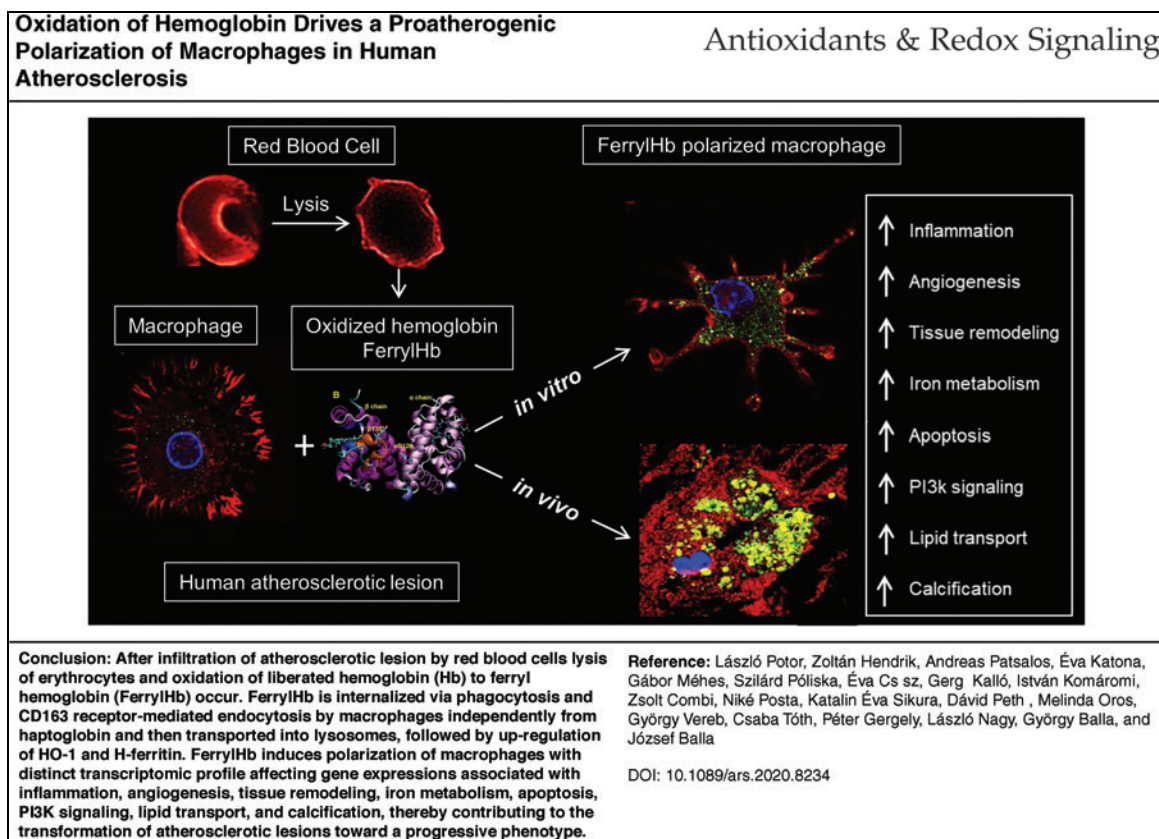†All these authors share the last authorship.
[i]ORCID ID (https://orcid.org/0000-0002-9022-4985).
[ii]ORCID ID (https://orcid.org/0000-0002-0437-4072).
[iii]ORCID ID (https://orcid.org/0000-0001-7923-2645).

remodeling, and vascularization. Targeted analysis of gene expression associated with calcification, apoptosis, and hemolytic-specific clusters indicated an increase in the severity of complicated lesions compared with atheroma. A 39% overlap in the differential gene expression profiles of human macrophages exposed to ferrylHb and the complicated lesion profiles was uncovered. Among these 547 genes, we found inflammatory, angiogenesis, and iron metabolism gene clusters regulated in macrophages.

Innovation and Conclusion: We conclude that oxidation of Hb to ferrylHb contributes to the progression of atherosclerosis *via* polarizing macrophages into a proatherogenic phenotype. *Antioxid. Redox Signal.* 35, 917–950.

Oxidation of Hemoglobin Drives a Proatherogenic Polarization of Macrophages in Human Atherosclerosis — Antioxidants & Redox Signaling

Conclusion: After infiltration of atherosclerotic lesion by red blood cells lysis of erythrocytes and oxidation of liberated hemoglobin (Hb) to ferryl hemoglobin (FerrylHb) occur. FerrylHb is internalized via phagocytosis and CD163 receptor-mediated endocytosis by macrophages independently from haptoglobin and then transported into lysosomes, followed by up-regulation of HO-1 and H-ferritin. FerrylHb induces polarization of macrophages with distinct transcriptomic profile affecting gene expressions associated with inflammation, angiogenesis, tissue remodeling, iron metabolism, apoptosis, PI3K signaling, lipid transport, and calcification, thereby contributing to the transformation of atherosclerotic lesions toward a progressive phenotype.

Reference: László Potor, Zoltán Hendrik, Andreas Patsalos, Éva Katona, Gábor Méhes, Szilárd Póliska, Éva Cs sz, Gerg Kalló, István Komáromi, Zsolt Combi, Niké Posta, Katalin Éva Sikura, Dávid Peth , Melinda Oros, György Vereb, Csaba Tóth, Péter Gergely, László Nagy, György Balla, and József Balla

DOI: 10.1089/ars.2020.8234

(*Color images are available online*).

Keywords: atherosclerosis, inflammation, vascular biology, vascular disease

Introduction

VULNERABLE PLAQUES, ESPECIALLY hemorrhaged lesions, contribute to a considerable extent to deaths (31%), according to the WHO. The complicated lesion is characterized by ruptures on the plaque surface and/or hemorrhage into the plaque (48). Intraplaque hemorrhage is also developed by the rupture of the neovascularized vessel, which is derived from the vasa vasorum (10, 46, 49). Carl von Rokitansky described for the first time that development of atheromatous plaque might be driven by the presence of blood elements, although plaque fissure is an underestimated source of intraplaque hemorrhage (17). Yuan *et al.* described that part of the damaged red blood cells (RBCs) are phagocytosed by macrophages, and exocytosis of the liberated iron triggers peroxidation of low-density lipoprotein (LDL) (76–78). Recently, Delbosc *et al.* demonstrated that intimal RBC infiltration is one of the initial triggers for foam cell formation

and intimal oxidation in early-stage atheroma (18). It was revealed that atherogenesis is an inflammation-promoted active process (59). Libby *et al.* reported that inflammation has a significant role in the complication of atherosclerosis, which is coordinated by immune cells (42, 43). Recent studies identified that macrophages have diverse phenotypes such as proinflammatory (''M1'') and alternatively polarized (''M2'') and consequently serve different functions in the progression of atherosclerosis (34, 47). Studies reported that heme, oxyHb, and inorganic iron alter macrophage polarization (12–14, 21, 68). However, a linear causal relationship between intralesional bleeding, macrophage polarization, and complex lesion formations has not been established yet.

It was shown that plaque materials with oxidative properties exhibit cytocidal effects and it was also observed that lysis of RBCs occurs followed by hemoglobin (Hb) release in the hemorrhagic plaques (51). Oxidation of Hb was found to

Innovation

A novel anti-ferrylHb monoclonal antibody was developed to explore the fate of hemoglobin (Hb) in hemorrhaged atherosclerotic lesion and the role of ferrylHb in the progression of atherosclerosis. In human atherosclerotic plaques, $\beta1Cys93$, $\beta1Cys112$, and $\beta2Cys112$ oxidation and a novel oxidation hotspot, $\alpha1Cys104$, were revealed in globin. Mechanisms of ferrylHb uptake by macrophages were uncovered utilizing stimulated emission depletion nanoscopy. Transcriptomic profile was determined; genes and pathways during the progression of atherosclerosis related to ferrylHb were presented using RNA-seq analysis on human carotid artery. In response to ferrylHb, reprograming of macrophages toward a proatherogenic phenotype was explored.

be oxidized to metHb (Fe^{3+}), and crosslinking of globin chains occurs *via* formation of dityrosins indicating the oxidation of heme to ferryl state and the subsequent formation of globin radicals at the site of hemorrhagic lesions (51). Importantly, ferrylHb (Fe^{4+}) is an elusive molecule that has a transient nature. FerrylHb autoreduces to metHb quite readily as part of the Hb pseudoperoxidative cycle damaging its globin chains. Protein radicals are formed and migrate to further damage the protein, including the oxidation of βCys-93 and dimerization (30, 54). FerrylHb has the propensity to also form free radicals in the alpha (αTyr-24, αHis-20, αTyr-42) and beta (βTyr-36, βTyr-130) chains of globins (19, 39, 56). Termination reactions of globin-centered radicals lead to the formation of globin-globin crosslinks resulting in Hb dimers, tetramers, and multimers.

A novel spectrophotometric method can be used to capture the spectral fingerprints of ferrylHb. Moreover, a novel and more accurate set of equations were established to improve the accuracy of methodologies in determining the transient ferrylHb species (44). In this study, to distinguish ferrylHb from metHb, we refer the globin-modified molecules as ferrylHb.

Similarly to heme, ferrylHb induces oxidant-mediated endothelial cell (EC) damage by supplying redox-active iron and therefore increases the production of reactive oxygen species (8, 9, 55). Oxidation of Hb impairs binding of the heme moiety to globin leading to release of heme, which exerts oxidative stress on EC (9) and triggers the lipid peroxidation of the LDL (7, 32, 55). Furthermore, ferrylHb acts as a proinflammatory agonist that targets vascular ECs. It induces monocyte adhesion on ECs by increasing the expression of adhesion molecules such as vascular cell adhesion molecule-1 (VCAM-1), E-selectin, and intercellular adhesion molecule-1 (ICAM-1) (55, 67).

Although oxidation of Hb is known to occur in ruptured atheromatous plaques, there has been no evidence whether it affects the transformation of lesions toward a progressive phenotype. Furthermore, it has not yet been elucidated what is the molecular mechanism of the clearance of ferrylHb, and if it is related to any cellular function. The aim of our study is to further explore the mechanism of Hb oxidation in the complicated atherosclerotic lesions, and to test whether oxidation of Hb to ferrylHb contributes to the progression of atherosclerosis *via* activation of macrophages.

Results

Hemorrhagic transformation of complicated atherosclerotic lesions

To reveal the pathophysiology of Hb oxidation in complicated lesions, we collected 122 carotid artery samples from patients who underwent endarterectomies from 2012 to 2021 and 13 carotid artery samples from cadavers of suicide or traumatic events for healthy controls in our studies. Conditions and comorbidities that occurred as well as medications are shown in Table 1. Specimens were classified according to AHA guidelines (69). Type IV (atheromatous) (Fig. 1A, middle panels) and type VI (complicated) lesions (Fig. 1A, right panels and Fig. 1B), as well as healthy carotid arteries (Fig. 1A, left panels), were investigated in our studies.

Macroscopic images (Fig. 1A, upper panel) and hematoxylin and eosin (H&E) staining (Fig. 1A, lower panel) of human carotid arteries showed clear evidence of acute intraplaque hemorrhage in the complicated lesion due to the presence of RBCs, compared with healthy vessel and atheroma. Cross section of the complicated lesion (Fig. 1B) exhibited a fresh hemorrhagic area (right upper panel) and hemorrhagic transformation without RBC infiltration (right lower panel). Staining for glycophorin A confirmed the presence of RBCs within the fresh hemorrhagic plaque (Fig. 2A, C). Costaining for CD68 (brown) and glycophorin A (red) demonstrated that $CD68^+$ cells were abundant in the hemorrhagic transformation region compared with the fresh hemorrhagic area of the complicated plaques (Fig. 2C). To follow the footsteps and clearance of Hb within the vessel wall, we used Prussian blue staining for iron as well as staining for ferritin and heme oxygenase-1 (HO-1) implicated in cardiovascular disease development (6) (Fig. 2A, D). In atheroma, cells lacked iron accumulation despite the enhanced H-ferritin expression in foam cells (Supplementary Fig. S1). Similarly, Prussian blue staining was not found in fresh hemorrhagic lesion (Fig. 2A, D). In contrast, a strong Prussian blue staining was found in the hemorrhagic transformation of complicated lesion (Fig. 2A, D). In certain parts of complicated lesions, not only iron was markedly accumulated but H-ferritin and HO-1 were also upregulated, intriguingly even in areas where RBCs were not readily detectable indicating the prior exposure to erythrocytes and Hb of that region (Fig. 2A, D). Importantly such an area exhibited significant infiltration with activated macrophages (CD68 and CPM positive) producing TNF-α and IL-1β (Fig. 2B, E). This unique posthemorrhagic lesion was designated as hemorrhagic transformation areas characterized by glycophorin A-negative but Prussian blue-positive staining with high expressions for H-FT ferritin and HO-1.

Since lysis of RBCs followed by severe oxidation of Hb leading to accumulation of ferrylHb occurs after plaque hemorrhage as a result of the interaction between erythrocytes and atheroma lipids (51, 55), we proposed that ferrylHb might trigger the progression of the disease *via* activating macrophages.

Development and characterization of a novel anti-ferrylHb monoclonal antibody

To follow the oxidation of Hb and to determine the fate of ferrylHb, we raised a novel mouse monoclonal antibody against human ferrylHb (anti-ferrylHb) as described in the Methods section. To identify the epitope of ferrylHb for the

TABLE 1. DATA OF PATIENTS WITH CAROTID ENDARTERECTOMY AND HEALTHY VOLUNTEERS

Data of patients with carotid endarterectomy	
Sampling period (year)	From 2012 to January 2021
Total sample number	A total of 78 were used for histology, 57 were used for spectrophotometric analysis, proteomic analysis, biochemical examination, molecular biology studies, RNA-sequencing
Gender	47 Females (35%), 88 males (65%)
Age	44–85 Years (average: 67.8 years, SD: 9.6 years)
Comorbidities and conditions that occurred in more than three patients	Hypertension (94%); peripheral artery disease (81%); ischemic heart disease (77%); obesity (62%); brain lacunar infarction (42%); type 2 diabetes mellitus (NIDDM; 38%), stroke (ischemic and hemorrhagic; 35%); hyperlipidemia (27%); coronary stent implantation (27%); myocardial infarction (23%); COPD (23%); hypothyroidism (19%), heart surgery—CABG (18%); bronchial asthma (15%); aortoiliac bypass surgery (12%); severe CKD (GFR <30; 12%); heart surgery—artificial aortic valve implantation (included TAVI; 8%); pacemaker implantation (8%)
Most frequent medications	Acetylsalicilic acid (91%); antacids (81%); beta-blocker (51%); diuretics (49%); allopurinol (42%); clopidogrel (42%); calcium channel blocker (40%); ACE inhibitor or ATII receptor antagonists (39%); statins (37%); alpha 1-receptor blocker (27); oral antidiabetic drugs (except insulin; 26%); warfarin or acenocoumarol (19%); citalopram (10%); carbamazepine (10%); piracetam (10%); insulin and insulin analogues (9%); folic acid (9%); levothyroxine (9%); alprazolam (9%); ipratropium-bromid (6%)
Data of healthy blood donor volunteers	
Sampling period (year)	From 2012 to January 2021
Total volunteer number	7
Total sample number	26
Gender	7 Males (100%)
Age	25–62 Years (average: 42.5 years, SD: 13 years)

CABG, coronary artery bypass graft; CKD, chronic kidney disease; COPD, chronic obstructive airway disease; GFR, glomerular filtration rate; NIDDM, non-insulin-dependent diabetes mellitus; SD, standard deviation; TAVI, transcatheter aortic valve implantation.

specific monoclonal anti-ferrylHb antibody, we used complex enzymatic digestions followed by matrix-assisted laser desorption ionization-time of flight (MALDI-TOF), liquid chromatography with tandem mass spectrometry (LC-MS/MS), and selective reaction monitoring (SRM)-based targeted proteomics. Trypsin- and Glu-C-digested peptides, respectively, were analyzed by mass spectrometry. First an MALDI-TOF analysis was done and in the case of trypsin digestion, a fragment with 1275.5 m/z value was identified (Supplementary Fig. S2A). This mass corresponds to the theoretical peptide LLVVYPWTQR at positions 32–41 of the beta subunit (theoretical mass: 1274.7). If we used Glu-C digestion and analyzed the peptides that remained on the antibody binding site by MALDI-TOF, the fragment with 2097.7 m/z value was found (Supplementary Fig. S2B) corresponding to the ALGRLLVVYPWTQRFFE peptide at positions 28–44 of the beta subunit (theoretical mass: 2095.1). This peptide fully overlaps with the tryptic peptide, thus confirming that the LLVVYPWTQR peptide contains the epitope of the antibody. To confirm the MALDI-TOF results, LC-MS/MS and SRM-based targeted proteomic experiments were applied. Both experiments confirmed the presence of LLVVYPWTQR peptide in the sample eluted from the beads (Supplementary Fig. S2C, D, and G). The characteristic dimeric "wild-type" and Tyr36 radical forms of α,β Hb structures, saved from the last frames of the molecular dynamics trajectories are shown (Supplementary Fig. S2E, F). It is immediately apparent from Supplementary Figure S2 that the Tyr36 residue and residues in its immediate vicinity of the β chain are significantly less solvent-exposed at the wild-type structures than at the corresponding structures with Tyr radicals. It can be observed in this Supplementary Figure S2 as well that the Tyr36 of β

chain forms a hydrogen bond with the Asp127 of the α chain, that is, contributes to the interchain stabilization while the Tyr36 radical does not.

Hb oxidation hotspots in human complicated lesions

Multiple evidence indicates that βCys93 is an important hotspot of free radical-induced oxidation in Hb (3, 30, 54). To study the oxidative modification of cysteines, we examined Hb derived from complicated lesions of carotid arteries with mass spectrometry. The oxidative events targeting Cys (oxidation and trioxidation of Cys) were examined and we detected the oxidation of Hb β1Cys93. Furthermore, β1Cys112 and β2Cys112 (33) were confirmed and α1Cys104 was revealed as a novel oxidation hotspot (Fig. 3 and Supplementary Fig. S3).

The oxidation of Hb and generation of the ferryl form are reflected by the presence of crosslinked Hb, a hallmark of ferrylHb. Western blot analysis of human carotid arteries with hemorrhage identified Hb dimers, tetramers, and multimers as a sign of globin radical formation and covalent crosslinking of globin chains (Fig. 4A). To further confirm the presence of ferrylHb in human complicated lesions, immunoprecipitation of ferrylHb was performed on healthy arteries ($N=3$), atheroma plaques ($N=3$), and hemorrhaged plaques ($N=3$). As shown in Figure 4B, the accumulation of ferrylHb was detected only in human complicated lesions. Spectrophotometric analysis was also applied to quantify ferrylHb and metHb in human complicated lesion (44). As the spectrophotometric analysis revealed 55% of the total Hb was ferrylHb, 39% was metHb, 1.4% was oxyHb, and the rest was ferrichrome in complicated carotid arteries (Fig. 4C).

Furthermore, we wondered which constituents of the atherosclerotic plaque might be responsible for Hb oxidation. To
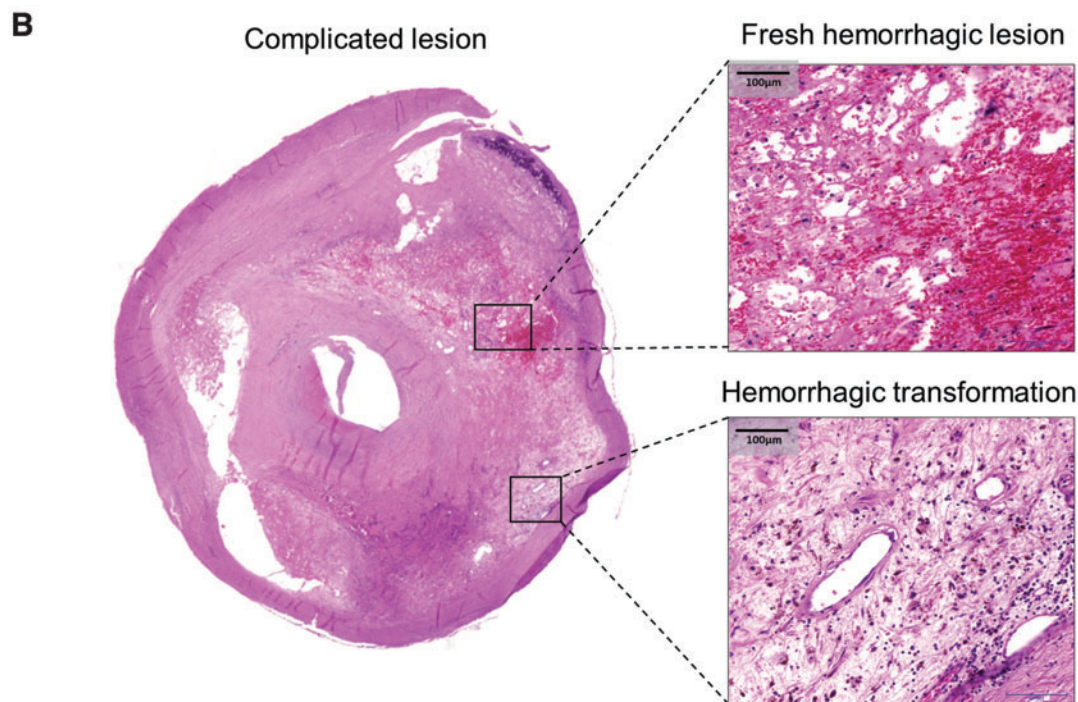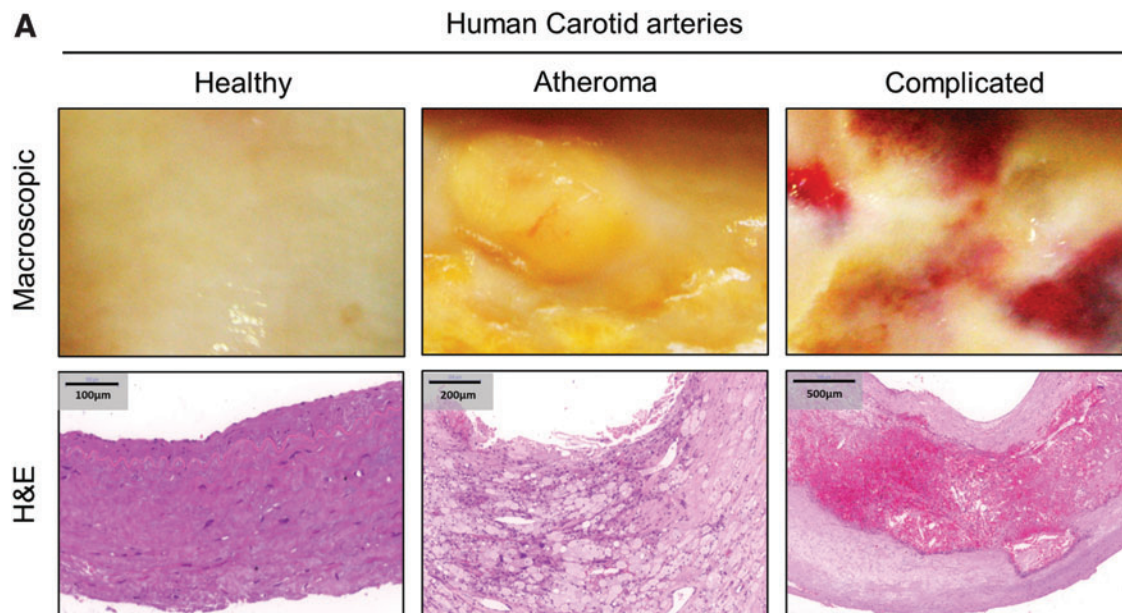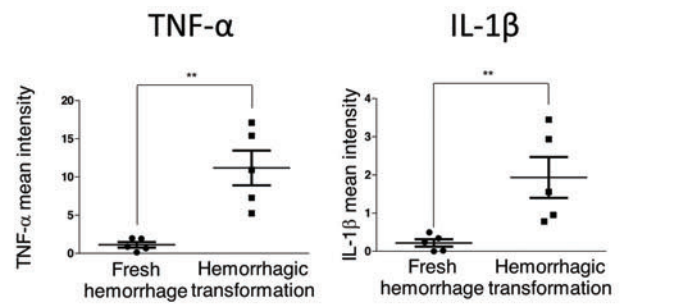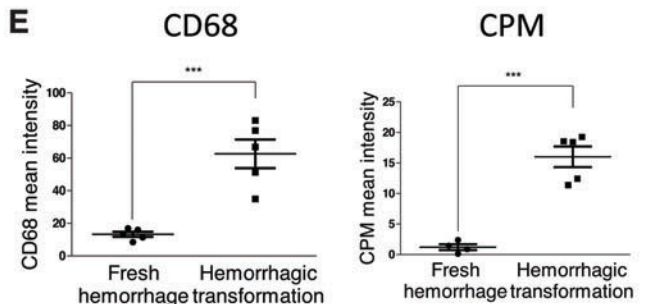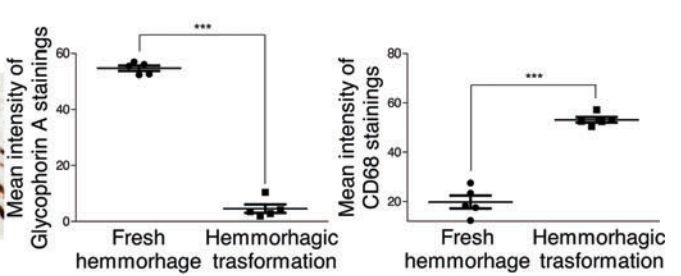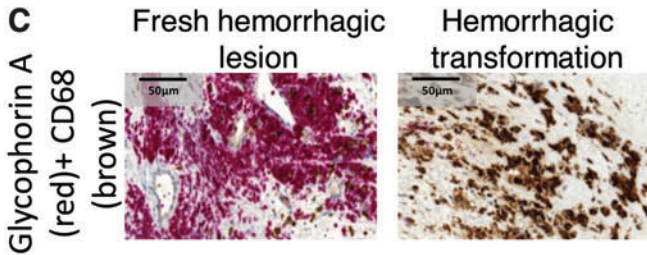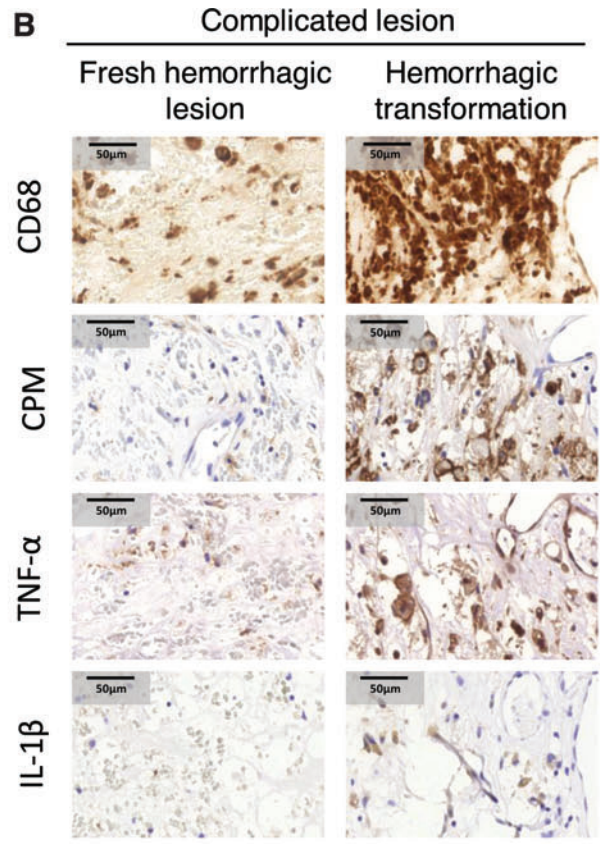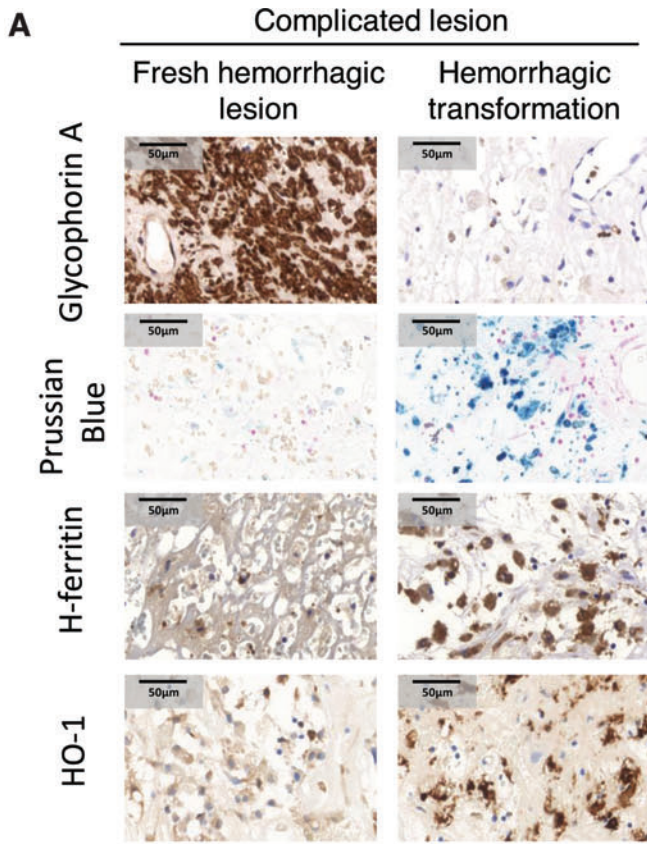
FIG. 1.   Fresh hemorrhage and hemorrhagic transformed area in human complicated plaque of the carotid artery.
(A) Segmental cross sections of a carotid artery demonstrating healthy area and atheromatous and complicated lesions. Macroscopic appearance (**A**, *upper panel*) and H&E staining (**A**, *lower panel*) are shown. **(B)** Typical view of an atherosclerotic human carotid artery (*left panel*, 5×magnification) featured by a fresh hemorrhagic lesion (*upper-right panel*) and hemorrhagic transformation (*lower-right panel*) within the same plaque area (H&E staining). Scale bars shown in the images represent 100, 200, or 500 μm. H&E, hematoxylin and eosin. Color images are available online.

FIG. 2.   Cellular responses in human complicated plaque of the carotid artery. (A, B) The area of a fresh hemorrhagic region (**A, B,** *left column*) was compared with a hemorrhagic transformed region (**A, B,** *right column*) using immunohistochemistry. Glycophorin A positivity demonstrates intact red blood cells (fresh hemorrhage) within a lesion, whereas Prussian blue indicates iron accumulation (hemosiderin) in the hemorrhagic transformed area. The presence and activation of macrophages are indicated by markers of CD68, carboxypeptidase M/CPM, TNF-α, and IL-1β (at 100×magnification). **(C)** CD68 and glycophorin A costaining was performed on complicated lesions. Images of fresh hemorrhagic area (*left image*) and hemorrhagic transformed region (*right image*) were shown. The mean intensity of CD68 and glycophorin A stainings was calculated using ImageJ software ($N = 5$). Heme-responsive proteins such as HO-1 and H-ferritin are demonstrated. **(C–E)** Quantitative analysis of immunohistochemical stainings of tissue sections was performed using ImageJ software ($N = 5$). Scale bars shown in the images represent 50 μm. **$p < 0.01$; ***$p < 0.001$. HO-1, heme oxygenase-1. Color images are available online.
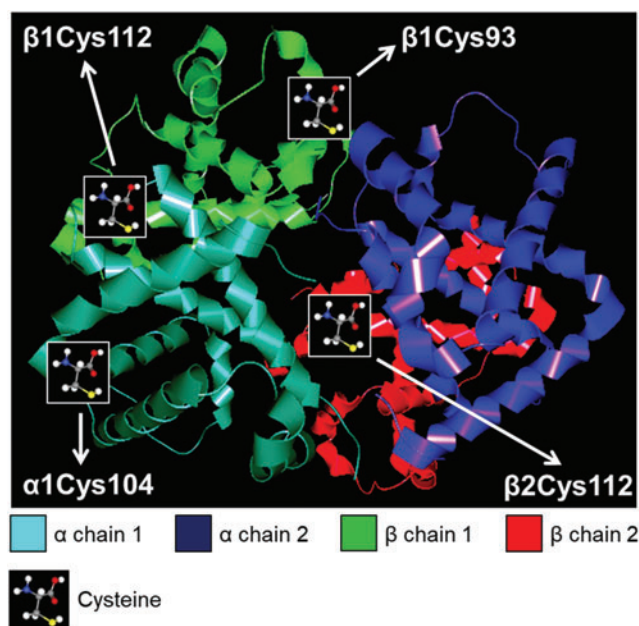
A Complicated lesion

Fresh hemorrhagic lesion — Hemorrhagic transformation

Glycophorin A

Prussian Blue

H-ferritin

HO-1

B Complicated lesion

Fresh hemorrhagic lesion — Hemorrhagic transformation

CD68

CPM

TNF-α

IL-1β

C

Glycophorin A (red) + CD68 (brown)

Fresh hemorrhagic lesion — Hemorrhagic transformation

Mean intensity of Glycophorin A stainings ***
Fresh hemorrhage — Hemmorhagic trasformation

Mean intensity of CD68 stainings ***
Fresh hemmorhage — Hemmorhagic trasformation

D

Glycophorin A — Glycophorin A mean intensity ***
Fresh hemorrhage — Hemorrhagic transformation

Prussian Blue — Prussian blue mean intensity ***
Fresh hemorrhage — Hemorrhagic transformation

H-ferritin — H-ferritin mean intensity **
Fresh hemorrhage — Hemorrhagic transformation

HO-1 — HO-1 mean intensity **
Fresh hemorrhage — Hemorrhagic transformation

E

CD68 — CD68 mean intensity ***
Fresh hemorrhage — Hemorrhagic transformation

CPM — CPM mean intensity ***
Fresh hemorrhage — Hemorrhagic transformation

TNF-α — TNF-α mean intensity **
Fresh hemorrhage — Hemorrhagic transformation

IL-1β — IL-1β mean intensity **
Fresh hemorrhage — Hemorrhagic transformation

FIG. 3. Oxidation hotspots of globin in human complicated lesion. Trypsin-digested human complicated lesion ($N = 5$) was utilized for LC-MS/MS analysis. The image presents the location of Cys oxidation in the Hb chains. Hb was visualized with CAVER Analyst 2.0 software using PDB entry 1BUW. Hb, hemoglobin; LC-MS/MS, liquid chromatography with tandem mass spectrometry. Color images are available online.

answer this question, *in vitro* models were set up to generate ferrylHb. We used conventional oxidants such as hydrogen peroxide (H_2O_2), lipid hydroperoxides (LOOH), as well as substances, oxidized LDL (oxLDL) or oxidized plaque lipid (oxPL), which could be found in the atheroma plaques. We demonstrated that all the oxidative reagents triggered the formation of Hb dimers, tetramers, and multimers as identified by sodium dodecyl-sulfate-polyacrylamide gel electrophoresis (SDS-PAGE) (Fig. 4D). A similar phenomenon was also observed using our anti-ferrylHb antibody on a native gel (Fig. 4E). As the spectrophotometric analysis revealed, the incubation of RBCs with LOOH or oxPL initiated the lysis of the cells and subsequently the oxidation of liberated Hb (Supplementary Fig. S4A). Anti-Hb antibody Western blot analysis of the lysed erythrocytes exposed to LOOH and oxPL demonstrated the generation of Hb dimers, which signifies the presence of ferrylHb (Supplementary Fig. S4B). The presence of ferrylHb was also confirmed by using the anti-ferrylHb antibody for the same samples (Supplementary Fig. S4C).

Next, we tested whether cells promote Hb oxidation as well. As we exposed oxyHb to macrophages, a rapid extracellular formation of ferrylHb occurred. Western blot analysis indicated the formation of ferrylHb in the supernatant of cell culture even after 1 h of exposure (Fig. 9A). Moreover, accumulation of ferrylHb was observed within the extracellular matrix as demonstrated by ferrylHb staining (Fig. 9B).

FerrylHb uptake by macrophages in hemorrhaged human carotid arteries via *phagocytosis and CD163 receptor-mediated endocytosis*

Staining tissues of human carotid arteries with the anti-ferrylHb antibody revealed both intracellular and extracel-

lular localizations of oxidized Hb in areas of chronic hemorrhagic transformation (Figs. 5, 6, and 7E). Control region (not stained for ferrylHb) and isotype control antibody staining of complicated lesion (Supplementary Fig. S5) indicates the specificity of ferrylHb staining (Fig. 5A, B; square c). To identify cells taking up ferrylHb, we performed double staining for a macrophage marker (CD68) and ferrylHb on the same specimens. We found that ferrylHb-positive cells were also CD68 positive (Figs. 5F and 6). Moreover, the internalization of ferrylHb was accompanied by upregulation of IL-1β and TNF-α in macrophages positive for CD68, as shown in Figure 6.

Since we demonstrated that in case of hemorrhagic plaque transformation ferrylHb is localized inside the macrophages together with elevated levels of IL-1β and TNF-α, we established an *in vitro* model to assess the effect of ferrylHb on macrophages. After exposure of cells to ferrylHb or oxyHb, samples were stained for the lysosome marker (lysosomal-associated membrane protein 1 [LAMP-1]), cytoskeleton (F-actin), nucleus (Hoechst), and ferrylHb (Fig. 7A). Confocal images visualized increased the signal of LAMP-1 after ferrylHb treatment (Fig. 7A, second column). We also observed that ferrylHb exposure changed the morphology of the cells (Fig. 7A). To track the uptake and the pathway of the ferrylHb inside the cells, we took super-resolution images of the macrophages with stimulated emission depletion (STED) nanoscopy. We revealed that macrophages engulfed the ferrylHb in actin-lined phagocytic cups at the end of the long thin pseudopodias (Fig. 7C). In addition, ferrylHb accumulated inside the LAMP-1-positive lysosomes (Fig. 7D). To confirm this finding, we isolated lysosomes from macrophages exposed to ferrylHb and performed Western blot analysis for LAMP-1 and ferrylHb. As shown in Figure 7E, ferrylHb was detected within the LAMP-1-positive lysosomes.

As previously demonstrated, ferrylHb provokes the rearrangement of actin cytoskeleton in ECs (67). The clearance function of macrophages is driven by actin polymerization (2). Here we showed that pseudopodia extension and filopodium formation have occurred during phagocytosis of ferrylHb in macrophages. Therefore, we examined whether inhibition of actin polymerization with latrunculin A (LAT A) and with latrunculin B (LAT B) may attenuate ferrylHb uptake by macrophages (Fig. 8). We found that both inhibitors induced characteristic morphological change of macrophages as reflected by the rounded cell shape. Importantly, both LAT A and LAT B suppressed the uptake of ferrylHb by macrophages (Fig. 8). Interestingly, in these experimental conditions where actin polymerization was inhibited, ferrylHb was accumulating outside of the cells, on the surface of macrophages (Fig. 8D). These studies indicate that phagocytosis is responsible for the uptake of ferrylHb.

Next, we asked whether ferrylHb might have a specific receptor on the surface of macrophages in the hemorrhaged complicated lesion. It is well established that the Hb-haptoglobin complex is taken up by the macrophage scavenger receptor CD163 (37). It is also known that CD163 exhibits low binding activity for native Hb or chemically altered Hb forms (62). Therefore, we tested if CD163 might act as a receptor for ferrylHb being abundant in the complicated lesion. Gene induction and protein expression analysis of human healthy carotid arteries, atheromas, and complicated atherosclerotic plaques proved that CD163 was
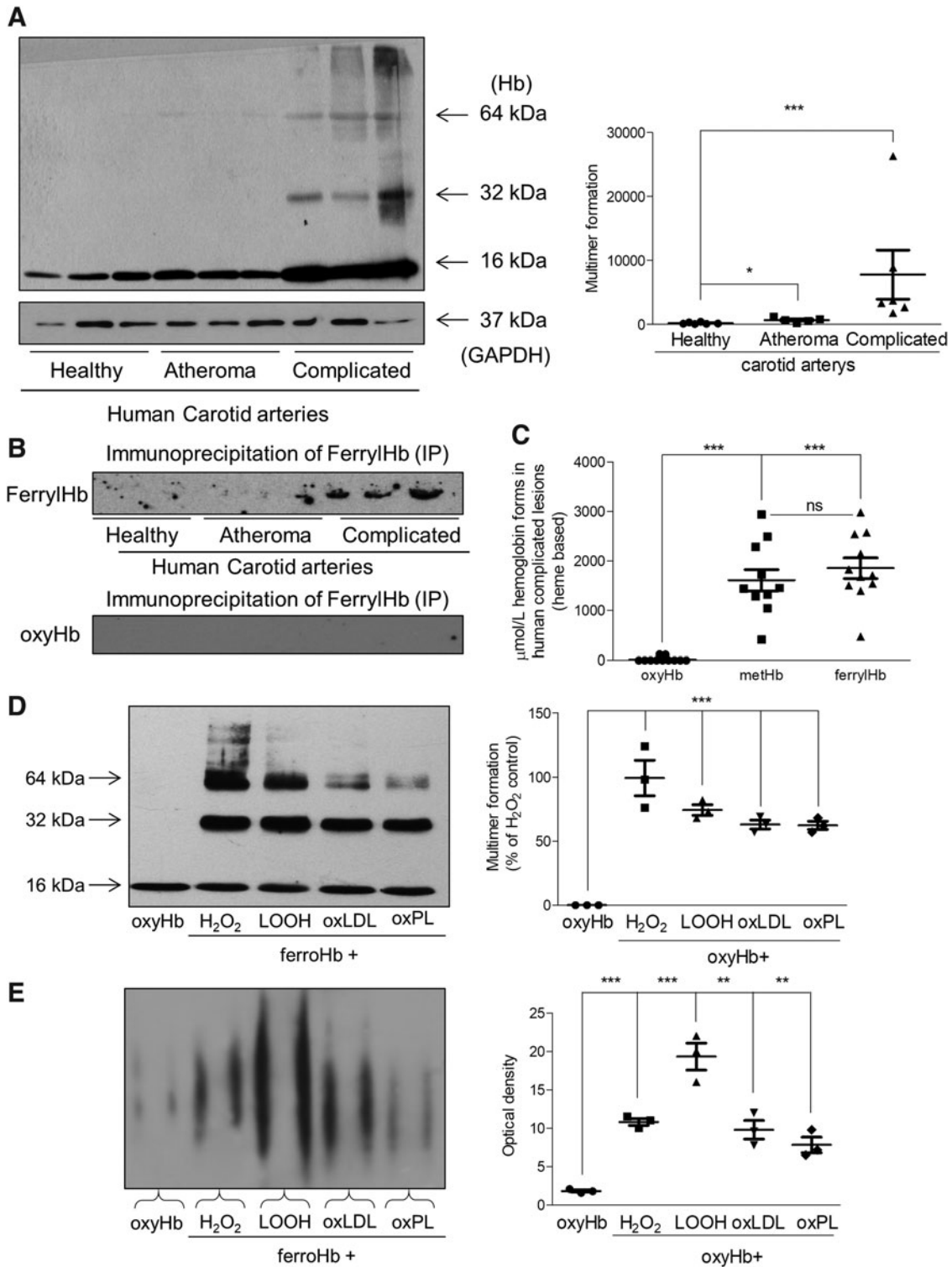
FIG. 4. Formation of ferryl hemoglobin and characterization of monoclonal anti-ferryl hemoglobin antibody. (**A,** *left panel*) Representative Western blot showing Hb expression in carotid artery tissue lysates (20 μg/lane; $N = 3$/group). (**A,** *right panel*) Quantification of multimer formation is shown ($N = 6$/group). (**B,** *upper panel*) Immunoprecipitation of oxidized Hb by ferrylHb was performed on healthy arteries ($N = 3$), atheromatous plaques ($N = 3$), and complicated lesions ($N = 3$). For control (**B,** *lower panel*) oxyHb and anti-ferrylHb were used ($N = 3$; 15 μL/lane; $N = 3$/group). (**C**) OxyHb, metHb, and ferrylHb species were determined by spectrophotometric analysis in human complicated lesions ($N = 11$). (**D, E**) OxyHb (5 μM) was incubated with H_2O_2 (50 μM); LOOH (25 μM); oxLDL (100 μg/mL); or oxPL (500 μg/mL). Samples (500 ng Hb) were subjected to (**D**) SDS-PAGE or (**E**) native gel electrophoresis, and Hb and ferrylHb species were detected by Western blotting ($n = 3$). (**D**) Quantification of multimer formation and (**E**) optical density are shown. $^*p < 0.05$; $^{**}p < 0.01$; $^{***}p < 0.001$ compared with nontreated Hb. H_2O_2, hydrogen peroxide; LOOH, lipid hydroperoxides; oxLDL, oxidized low-density lipoprotein; oxPL, oxidized plaque lipid; SDS-PAGE, sodium dodecyl-sulfate polyacrylamide gel electrophoresis.

pronounced in complicated lesions (Fig. 10A, B). Using the anti-ferrylHb antibody in the immunofluorescence examination of complicated lesions revealed that the increased expression of CD163 occurred in those cells that were stained for ferrylHb as well (Fig. 10C, D). Using STED nanoscopy on the human atherosclerotic samples indicated that ferrylHb and CD163 were colocalized in macrophages of transformed hemorrhagic plaques (colocalization rate: 98.65% ± 1.46%) (Fig. 10C–E).

To mimic this *in vivo* finding, we exposed human macrophages to ferrylHb in cell culture. Immunofluorescent staining and three-dimensional images of Z-Stack-STED nanoscopy presented a strong colocalization of ferrylHb and CD163 in macrophages (Fig. 11A–D). Importantly, CD163 expression was enhanced in cells treated with ferrylHb at both RNA and protein levels (Fig. 11E, F) as it was similarly observed in the complicated lesion. To provide evidence that ferrylHb uptake occurs *via* CD163, we used CD163 small interfering RNA (siRNA) to knock down *CD163* gene expression in macrophages. For control, as shown in Figure 12 (second row), exposure of macrophages to ferrylHb exhibited strong intracellular staining. On the contrary, silencing *CD163* gene led to faint ferrylHb staining in macrophages (Fig. 12, third row). This study indicates that ferrylHb is also taken up *via* CD163 receptor-mediated endocytosis independently from haptoglobin.

Oxidation of Hb to ferrylHb was shown to be driven by lipid peroxide substances (oxLDL or oxPL) found in atherosclerotic plaques, but other oxidants derived from the resident cells, including macrophages, might facilitate Hb oxidation as well (Fig. 9A) promoting its uptake. As we expected, Hb uptake occurred after a 12-h lag when oxyHb was added to macrophage compared with ferrylHb (Fig. 9C). During this period of time, ferrylHb was formed from oxyHb in the supernatant of cells (Fig. 9A). Interestingly, the clearance of ferrylHb by macrophage from the extracellular matrix was observed (Fig. 9B).
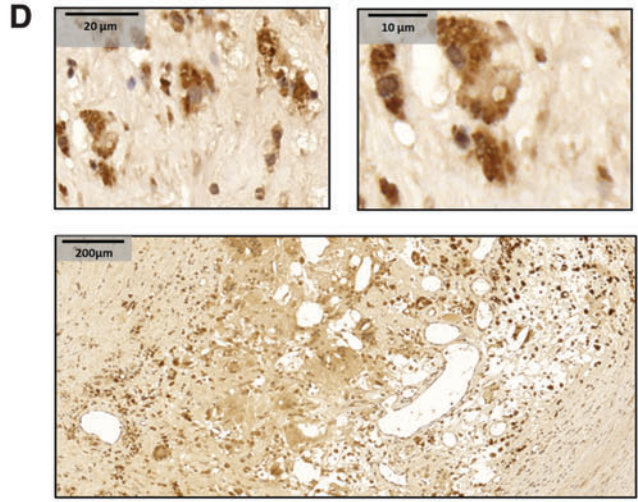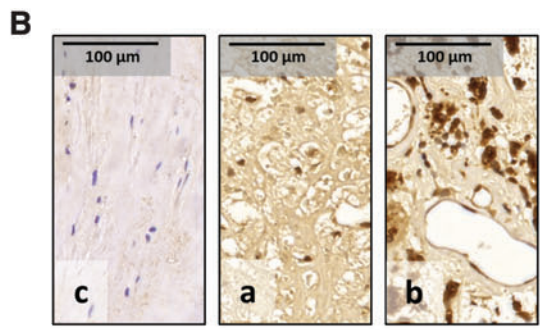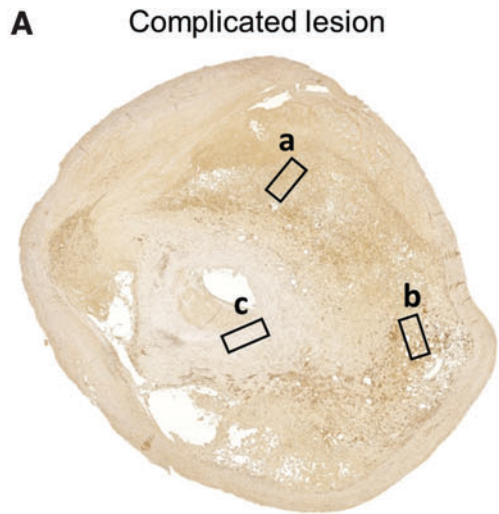
Human macrophages acquire a proinflammatory gene expression signature *in vitro upon exposure to ferrylHb*

Since proinflammatory cell phenotypes develop during hemorrhagic plaque transformation, we tested whether uptake of ferrylHb by human macrophages alters their polarization *in vitro*. RNA-seq analysis from vehicle- or ferrylHb-treated (for 8 h) macrophages revealed 1341 differentially
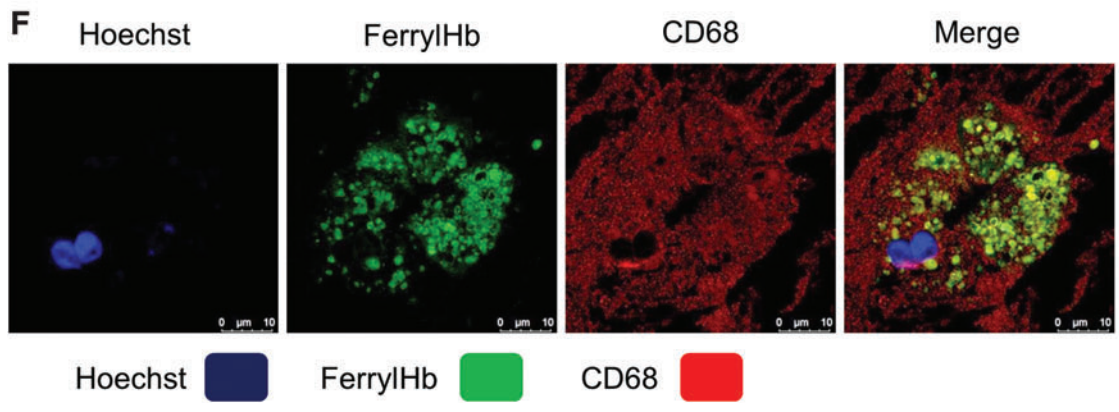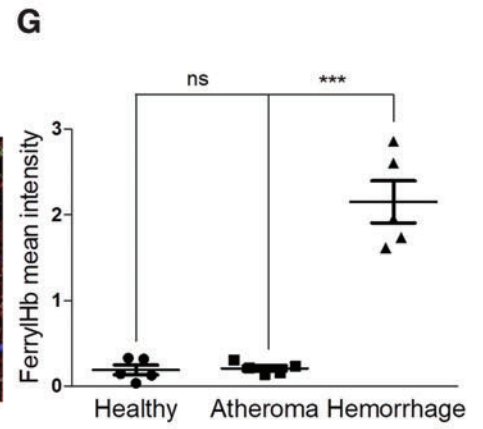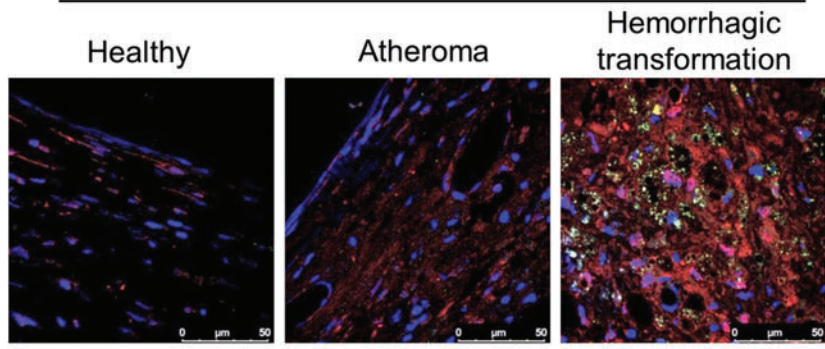
expressed (DE) genes (Supplementary Fig. S10A), with the top 50 shown in Figure 13A. Also, an unbiased investigation of the most affected cellular pathways associated with ferrylHb uptake in human macrophages was performed using the Gene Ontology (GO) Resource database (Supplementary Fig. S10B) (5, 70). Interestingly, ferrylHb treatment significantly affected genes associated with the activation of several proinflammatory pathways involving cell responses to tumor necrosis factor, interleukin-1, and lipopolysaccharide, as well as gene changes associated with phagocytosis and chemotaxis (Fig. 13B), all indicative of a potential acquisition of a proinflammatory phenotype. Indeed, several of the upregulated genes could be classified into known classical M1 polarizing gene clusters, including *IL-6*, *IL-1A*, *IL-1B*, *CXCL11*, *CXCL8*, *IDO1*, *TNF*, *STAT1*, and *CCL4* (Fig. 13A, B, left panel) (11, 16, 22). At the same time, several anti-inflammatory M2-polarization marker genes seem to be significantly altered by ferrylHb exposure indicative of a distinct transcriptomic signature that cannot be classified entirely into canonical M1 or M2 polarization states (Fig. 13B, right panel). We further validated these observations by performing real-time quantitative polymerase chain reaction (RT-qPCR) and Western blots on gene sets representative of the different polarization states. We found that ferrylHb treatment did increase the messenger RNA (mRNA) levels of inflammatory markers such as *IL-1β*, *TNF-α*, and *CXCL8*, in agreement with the RNA-seq findings (Fig. 13C). In contrast, the mRNA expression of the anti-inflammatory marker *CD209* was found to be decreased, while *IL-27RA* was elevated by exposure of ferrylHb (Fig. 13D).

The enhanced synthesis of IL-1β and TNF-α was also confirmed at the protein level by Western blot analysis (Fig. 13E). Furthermore, the expression of genes involved in the catabolism of Hb was also assessed. In macrophages exposed to ferrylHb, oxyHb and heme exhibited an elevated level of HO-1 and ferritin. *HO-1* mRNA peaked at 8, 16, and 24 h after heme, ferrylHb, and oxyHb treatment, respectively (data not shown). Similar patterns were observed at the protein level with both HO-1 and H-ferritin being increased in human macrophages exposed to ferrylHb (Fig. 13E). MetHb was demonstrated to lose heme moieties more readily than ferrylHb (36). Therefore, we measured HO-1 mRNA and protein levels in macrophages exposed to oxyHb, metHb, and ferrylHb in fetal bovine serum (FBS)-free media at 4 h of exposure. Heme, metHb, and ferrylHb enhanced HO-1 at

FIG. 5. Ferryl hemoglobin is characteristic of the hemorrhagic transformed region localized extracellularly and within CD68$^+$ macrophages. (A) Fresh hemorrhagic region (*square a*), hemorrhagic transformed region (*square b*), and control region (*square c*) were demonstrated using ferrylHb immunohistochemistry on complicated lesions. **(B)** 100 × Magnification images demonstrated FerrylHb positivity of fresh hemorrhagic region (*square a*), hemorrhagic transformed region (*square b*), and control region (*square c*) of complicated lesions. **(C)** Quantitative analysis of ferrylHb immunohistochemical stainings of tissue sections was performed using ImageJ software (*N* = 5). **(D)** Intracellular (*upper panels*) and extracellular (*lower panel*) accumulation of ferrylHb is shown in hemorrhagic transformed area. **(E)** Segmental cross sections of a healthy carotid artery and atheromatous and hemorrhagic transformed lesions were shown. **(F)** High-magnification images demonstrated macrophages positive for both ferrylHb and CD68 in the hemorrhagic transformed lesions. Sections were stained with Hoechst 33258 for DNA (*blue*), an anti-ferrylHb antibody with Alexa Flour 488 secondary antibody for ferrylHb (*green*), and anti-CD68 antibody with Alexa Flour 647 secondary antibody for CD68 (*red*). Images were taken using Leica TCS SP8 gated STED-CW nanoscopy. Images were deconvolved using Huygens Professional software. Representative image, *N* = 5. **(G)** Fluorescence intensity for ferrylHb staining was calculated using ImageJ software (*n* = 5). Scale bars shown in the images represent 10, 20, 50, 100, or 200 μm. ***p < 0.001. CW, continuous wavelength; ns, not significant; STED, stimulated emission depletion. Color images are available online.

A Complicated lesion

B

C
FerrylHb mean intensity

Control region — Fresh hemorrhagic lesion — Hemorrhagic transformation

ns

***

***

D
20 μm
10 μm
200μm

E Human Carotid arteries

Healthy   Atheroma   Hemorrhagic transformation

G
FerrylHb mean intensity

ns   ***

Healthy   Atheroma   Hemorrhage

F
Hoechst   FerrylHb   CD68   Merge

Hoechst   FerrylHb   CD68

926
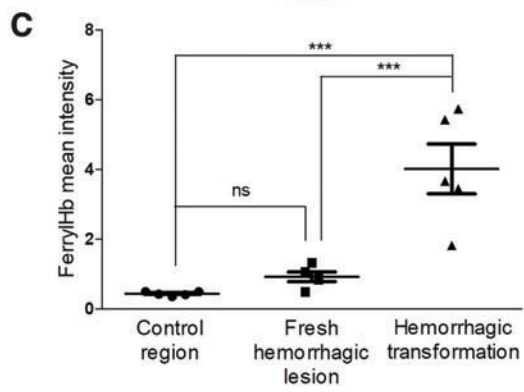
both mRNA and protein levels. Interestingly, the induction was more pronounced in cells exposed to ferrylHb compared with metHb. Furthermore, we observed a significantly less induction of HO-1 in cells exposed to oxyHb compared with ferrylHb (Supplementary Fig. S8).

It has been reported that depletion of CD163 upregulates CD36 expression and increases foam cell formation in M2-type macrophages (26). Since CD163 protein expression was elevated in macrophages exposed to ferrylHb, we assessed whether the CD36 protein expression was also altered in cells exposed to ferrylHb. As shown in Supplementary Figure S9, CD36 protein expression was increased by 1.4-fold in macrophages exposed to ferrylHb compared with nontreated cells.

Activation of phosphoinositide 3-kinase/hypoxia-inducible factor 1-alpha/vascular endothelial growth factor pathway in macrophages by ferrylHb

The phosphoinositide 3-kinase (PI3K)/hypoxia-inducible factor 1-alpha (HIF-1α)/vascular endothelial growth factor (VEGF) pathway drives the expression of proinflammatory cytokines (25, 29, 52, 64). Since RNA-seq analysis suggested that activation of PI3K signaling occured and angiogenesis was driven by induction of HIF-1α and VEGF in hemorrhagic lesion (Supplementary Fig. S11), we analyzed the phosphorylation of PI3K, protein expression of HIF-1α, and secretion of VEGF-A in macrophages exposed to ferrylHb. As shown in Figure 14A, phosphorylation of PI3K occurred in macrophages exposed to ferrylHb at 2 h. At this time point, phosphorylation of PI3K was not present in cells exposed to oxyHb (Fig. 14A). Next, we examined the protein expression of HIF-1α in macrophages exposed to heme, oxyHb, metHb, and ferrylHb at 24 h. We found that the expression of HIF-1α protein was stabilized by ferrylHb but not by heme, oxyHb, or metHb (Fig. 14B). Stabilization of HIF-1α was accompanied by enhanced secretion of VEGF-A (Fig. 14C).

Transcriptomic signatures of human complicated atherosclerotic plaques, atheromas, and healthy carotid arteries

To expand our investigations and identify the genes and pathways that differ among patients with complicated lesions, atheromas, and healthy arteries, RNA-seq analysis was performed on biopsies from these three groups. Despite the genetic variability usually found in human samples, complicated lesions and atheromatous samples had a distinct transcriptomic profile and biological replicates cluster to-

gether, when compared with healthy tissue segments (Fig. 15A). As shown in Figure 15B, a large number of transcripts were substantially and distinctly changed in atheromatous or complicated lesions compared with healthy samples (4237 and 6408 DE genes, respectively). Several of the top DE genes, (including *HO-1*, *CCL18*, macrophage markers such as *MS4A4A*, *LYZ*, and several members of the pathological matrix metallopeptidases and solute carrier family of transporters) changed in both atheromatous and complicated lesions although at a higher level and fold change in the complicated lesions (Fig. 15B). Unbiased investigation of the most affected cellular pathways associated with complicated lesions was performed using the GO Resource database (Supplementary Fig. S11). Interestingly, affected genes are primarily associated with macrophage and neutrophil activation (including nitric oxide, IL-1, TNF-α, IL-8, and IFN-γ regulated pathways), angiogenesis, and iron ion transport, in line with our histological observations. Other notable pathways affected in complicated lesions include gene changes associated with PI3K signaling, lipid transport, tissue remodeling, and artery development (Supplementary Fig. S11). Targeted analysis of gene expression associated with calcification, apoptosis, and hemolytic-specific clusters further suggests the increase in severity of complicated lesions compared with atheromatous (Fig. 15C). Interestingly, several inflammatory gene sets (Fig. 15D), including *NLRP3* (encodes inflammasome components), interleukins, and several TLRs, as well as several genes associated with iron metabolism (Fig. 15C, D), such as *BACH1*, *NRF2* (*NFE2L1*), *HO-1*, and ferritins (*FTL*, *FTH1*) among others, were associated with complicated plaques. These data demonstrate that complicated lesions can be distinguished at the transcriptomic level, involve several inflammatory and iron metabolism pathways, and likely account for the drastic phenotype differences in patients with atheroma and complicated lesions.

Lastly, we asked whether, and to what degree, the transcriptional changes observed in patients with complicated lesions are related to the exposure of macrophages to ferrylHb. By comparing the differential gene expression profiles of human primary macrophages from healthy donors treated with ferrylHb *in vitro* and the complicated/atheromatous lesion profiles we discussed above, we found a 39% overlap (Fig. 16A). To gain insight into the specific action of ferrylHb, gene expression profiles of human primary macrophages exposed to either ferrylHb or Hb and the profiles of complicated lesions were also compared. We found a 34.6%

FIG. 6. Ferryl hemoglobin-positive macrophages in carotid artery are positive for IL-1β and TNF-α. Cross sections of a healthy carotid artery and atheromatous and hemorrhagic transformed lesions were shown. **(A)** Images demonstrated macrophages positive for both CD68 and IL-1β in the atheromatous plaque and positive for ferrylHb, CD68, and IL-1β in the hemorrhagic transformed lesions. Sections were stained with Hoechst 33258 for DNA (*blue*), an anti-ferrylHb antibody with Alexa Flour 488 secondary antibody for ferrylHb (*green*), an anti-CD68 antibody with Alexa Flour 568 secondary antibody for CD68 (*yellow*), and an anti-IL-1β antibody with Alexa Flour 647 secondary antibody for IL-1β (*red*). **(B)** Images demonstrated macrophages positive for both CD68 and TNF-α in the atheromatous plaque and positive for ferrylHb, CD68, and TNF-α in the hemorrhagic transformed lesions. Sections were stained with Hoechst 33258 for DNA (*blue*), an anti-ferrylHb antibody with Alexa Flour 488 secondary antibody for ferrylHb (*green*), an anti-CD68 antibody with Alexa Flour 568 secondary antibody for CD68 (*yellow*), and an anti-TNF-α antibody with Alexa Flour 647 secondary antibody for TNF-α (*red*). Images were taken using Leica TCS SP8 gated STED-CW nanoscopy. Images were deconvolved using Huygens Professional software. Representative image, $N = 5$. **(C)** Fluorescence intensity for ferrylHb ($n = 17$), CD68 ($n = 20$), IL-1β ($n = 19$), and TNF-α ($n = 15$) staining was calculated using ImageJ software. $*p < 0.05$; $**p < 0.01$; $***p < 0.001$. Color images are available online.
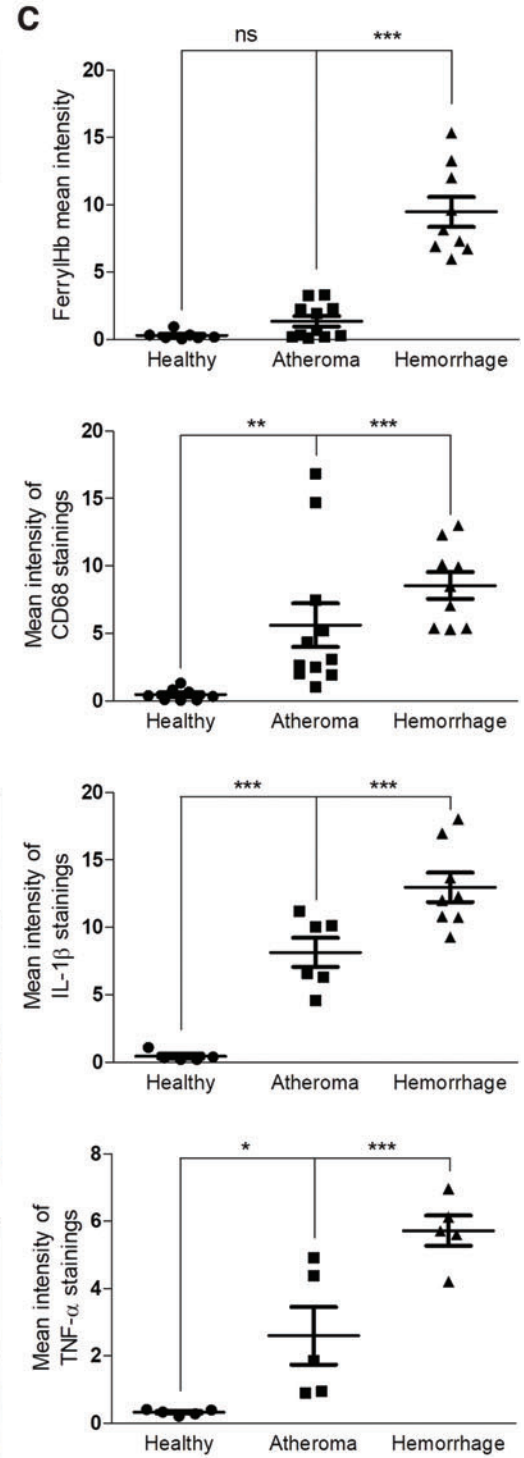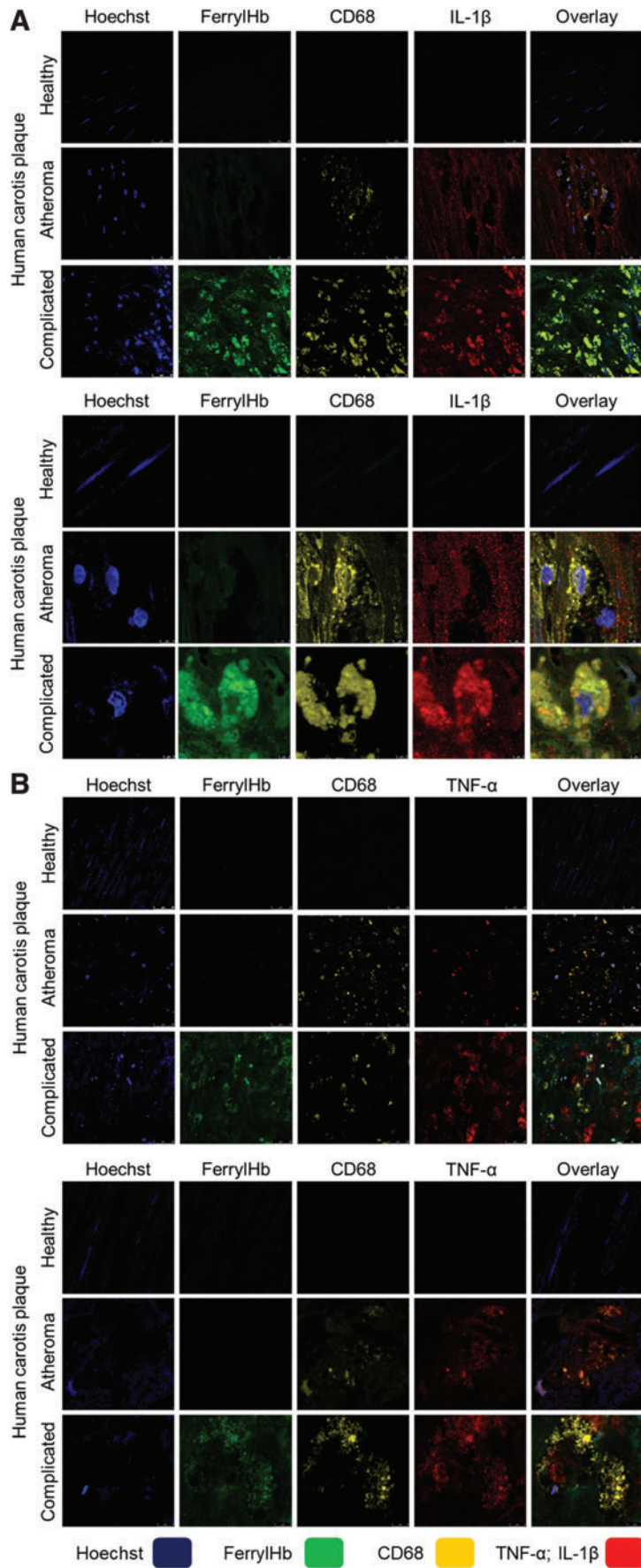
overlap, and among these 462 genes, 112 were exclusively regulated by ferrylHb and 350 that were controlled by both ferrylHb and oxyHb treatment, although not to the same degree (Supplementary Fig. S12A). Importantly, most of the gene expression changes induced by ferrylHb treatment were quantitatively and qualitatively comparable with the hemorrhaged patients' complicated lesion profile (Fig. 16B). The top genes changed in both human macrophages treated with ferrylHb and complicated lesions are depicted in the clustered heatmap in Figure 16C and D and include interleukins, metalloproteinases, interferon response factors, chemokine receptors, toll-like receptors and iron catabolism-related enzymes. These gene sets are likely to be responsible for the activation of pathways associated with immune cell activity and inflammatory cytokine signaling, as demonstrated by the GO enrichment analysis (Supplementary Fig. S12E). Further gene enrichment annotation analysis of the ferrylHb exclusive gene cluster (112 genes) revealed genes related to heme/iron degradation and transport (*ME1*, *STEAP4*, *ABCB6*), fat and smooth muscle cell differentiation (*ADIRF*, *AEBP1*), fatty acid and redox regulation (*TXN*), chemokines (*CCL8*, *CXCL6*), cytokine receptors (*IL17RB*, *LIFR*, *LTB*), cell cycle and apoptosis pathways (SQSTM1), wound healing and repair (*YAP1*, *IGF2*), subcellular calcium and other ion transport processes (*i.e.*, *ABCC6*, *CACNB3*, *WNK3*, *KCNMB1*, *KCNJ2*, *EPHB2*), as well as genes related to macrophage activation and inflammation (*S100A8*, *P2RX7*, *P2RY6*, *PTGER3*, *PLAC8*) pointing toward a functionally distinct function of the ferrylHb form. Genes within this annotation cluster also following the direction of the regulation seen in the complicated lesion profiles are shown in Supplementary Figure S12B, while genes included in the triple shared cluster (350 genes) following a similar magnitude of regulation are shown in Supplementary Figure S12C–E. GO pathway analysis of this shared cluster (350 genes) revealed several inflammatory and myeloid migration pathways (Supplementary Fig. S12E), including neutrophil and natural killer cell chemotaxis, regulation of cell death, response to interleukin-1, as well as nitric oxide and VEGF production. These data suggest that ferrylHb is a functionally distinct form of Hb and the gene expression changes induced by it in macrophages suggest that its formation in atherosclerotic lesions, as well as its uptake by recruited macrophages, is likely to promote the progression of the disease. Thus, mechanistically it acts *via* the rupture of the neovascularized vessel, and by polarizing macrophages into a proinflammatory-like phenotype.
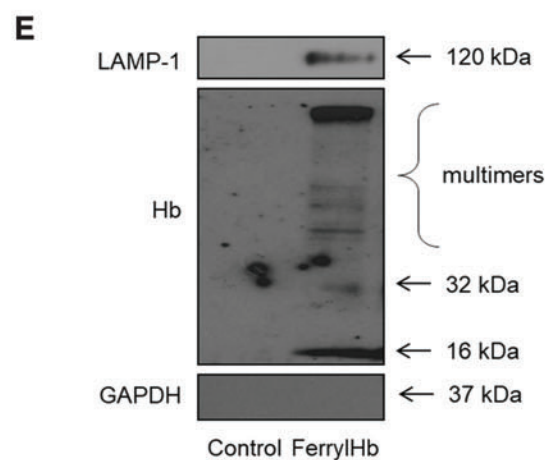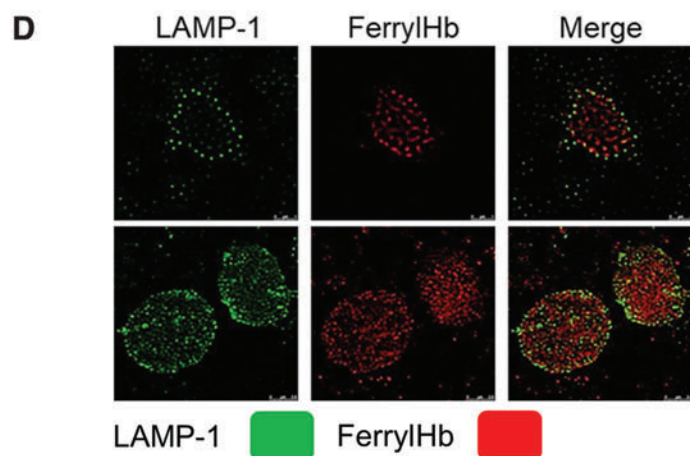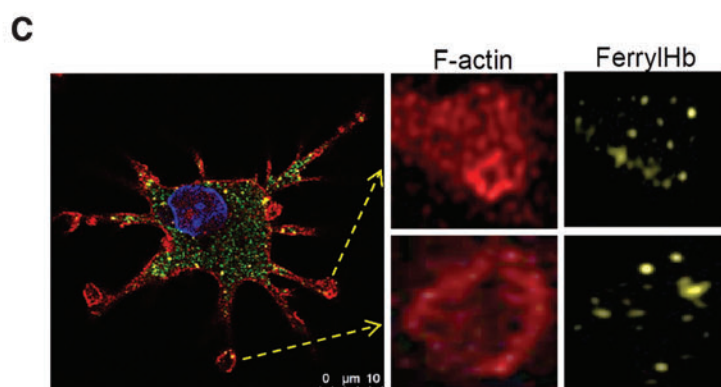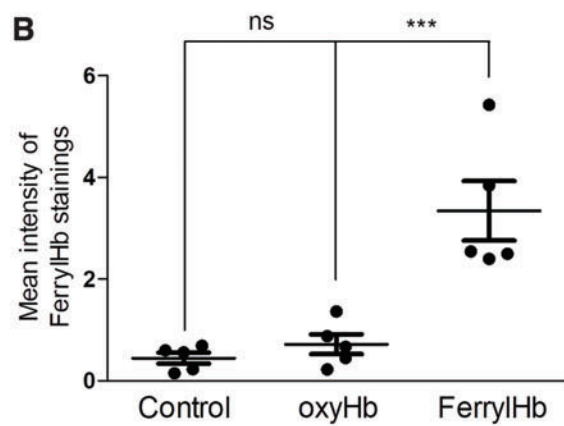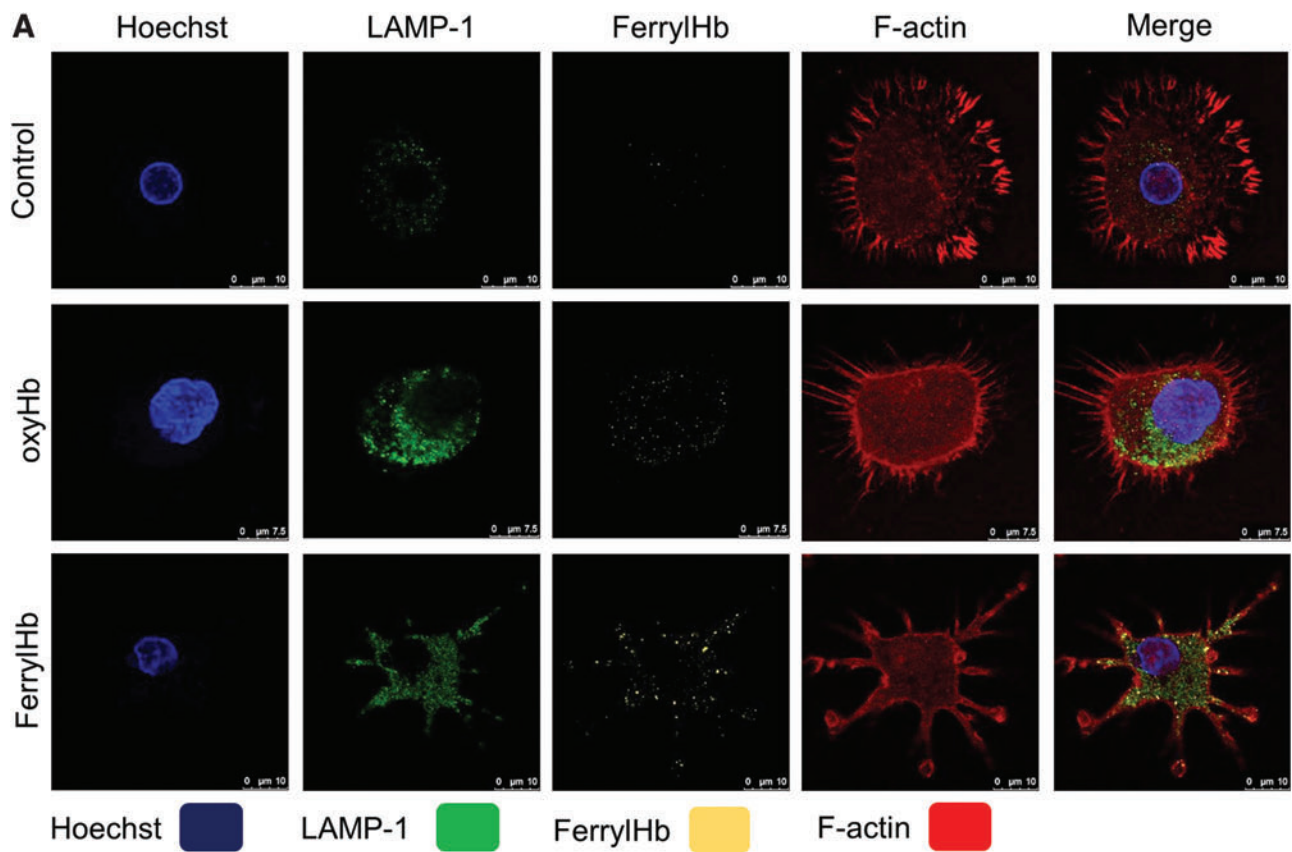
Discussion

Auto-oxidation of Hb leads to metHb generation and in the meanwhile superoxide anions are formed. Peroxides can trigger two-electron oxidation of Hb leading to the formation of ferrylHb, whereas the reaction of oxyHb with peroxides yields ferrylHb radical [Hb$^\bullet$+(Fe^{4+}=O^{2-})], in which the unpaired electron is associated with the porphyrin ring or the globin (4, 27, 28, 33, 53). The generated high-valence iron compounds are highly reactive intermediates that can decay in several ways (33, 57, 58).

While in RBCs, oxidation of Hb is inhibited by a highly effective antioxidant defense system (65) as RBCs enter the oxidative milieu of atherosclerotic lesions containing products of lipid peroxidation, such as LOOH, aldehydes, and carbonyls (40), they lyse and Hb is released (51). Hb once outside the protective environment of RBCs is prone to oxidation. Studying the interaction of Hb and atheroma lipids, we observed that severe oxidation of Hb leads to the generation of ferrylHb (Fig. 4 and Supplementary Fig. S4). Extracellular Hb is also oxidized to ferrylHb by macrophages (Fig. 9). Moreover, we revealed a significant accumulation of extracellular ferrylHb within human complicated atherosclerotic plaques (Fig. 5). Hb dimers, tetramers, and multimers were identified in the lesions (Fig. 4A) that were accompanied by the accumulation of dityrosine (51).

A novel oxidative pathway was previously revealed during the exposure of Hb to H$_2$O$_2$ by the Alayash group (33). It was demonstrated that generation of ferryl state in the heme moiety of Hb is accompanied by the formation of a protein-based ferryl radical that migrates to βCys93 and induces further oxidative changes and unfolding of the protein (3, 30). Therefore, we examined Hb derived from complicated lesions of human carotid arteries with mass spectrometry and observed oxidation of βCys93 residue in the complicated atherosclerotic lesion. Moreover, we confirmed the oxidation of β1Cys93, β1Cys112, and β2Cys112 and identified novel oxidation hotspot of Hb (α1Cys104) confirming the presence of transient ferrylHb species as part of the progression of atherosclerosis (Fig. 3 and Supplementary Fig. S3).

To study the fate of ferrylHb and the pathophysiology of Hb oxidation in human complicated lesion, we produced a monoclonal anti-ferrylHb antibody. MALDI-TOF analysis, MS/MS-based protein identification, and SRM-based targeted proteomics were used to identify that the LLVVYPWTQR sequence at positions 31–40 of the beta subunit contains the target epitope of the anti-ferrylHb antibody. Molecular

FIG. 7. Ferryl hemoglobin is ingested by macrophages. (A–D) Macrophages grown on coverslips were exposed to oxyHb (10 μM), ferrylHb (10 μM), or growth medium for 12 h. Cells were stained with Hoechst 33258 for DNA (*blue*), an anti-LAMP-1 antibody with Alexa Fluor 488 secondary antibody for lysosomes (*green*), an anti-ferrylHb antibody with Alexa Flour 568 secondary antibody for ferrylHb (*yellow*), and iFluor 647 phalloidin for cytoskeleton (*red*). **(B)** Fluorescence intensity for ferrylHb staining was calculated using ImageJ software (*n*=5). **(C)** Actin-lined phagocytosis of the ferrylHb was shown. **(A, B)** Multicolor confocal imaging was acquired with a Leica TCS SP8 microscope. **(D)** Localization of the ferrylHb (for better contrast the color of ferrylHb was changed from *yellow* to *red*) inside the lysosomes (*green*) was demonstrated using Leica TCS SP8 gated STED-CW nanoscopy. Images were deconvolved using Huygens Professional software. Representative images are shown (*n*=5). Scale bars shown in the images represent 0.5, 0.75, and 10 μm. **(E)** Macrophages were exposed to ferrylHb (10 μM) or growth medium for 24 h. Six micrograms of protein of isolated lysosomes was analyzed by Western blot. Expressions of LAMP-1, Hb, and GAPDH were assessed (*n*=3). ***$p < 0.001$. GAPDH, glyceraldehyde 3-phosphate dehydrogenase; LAMP-1, lysosomal-associated membrane protein 1. Color images are available online.
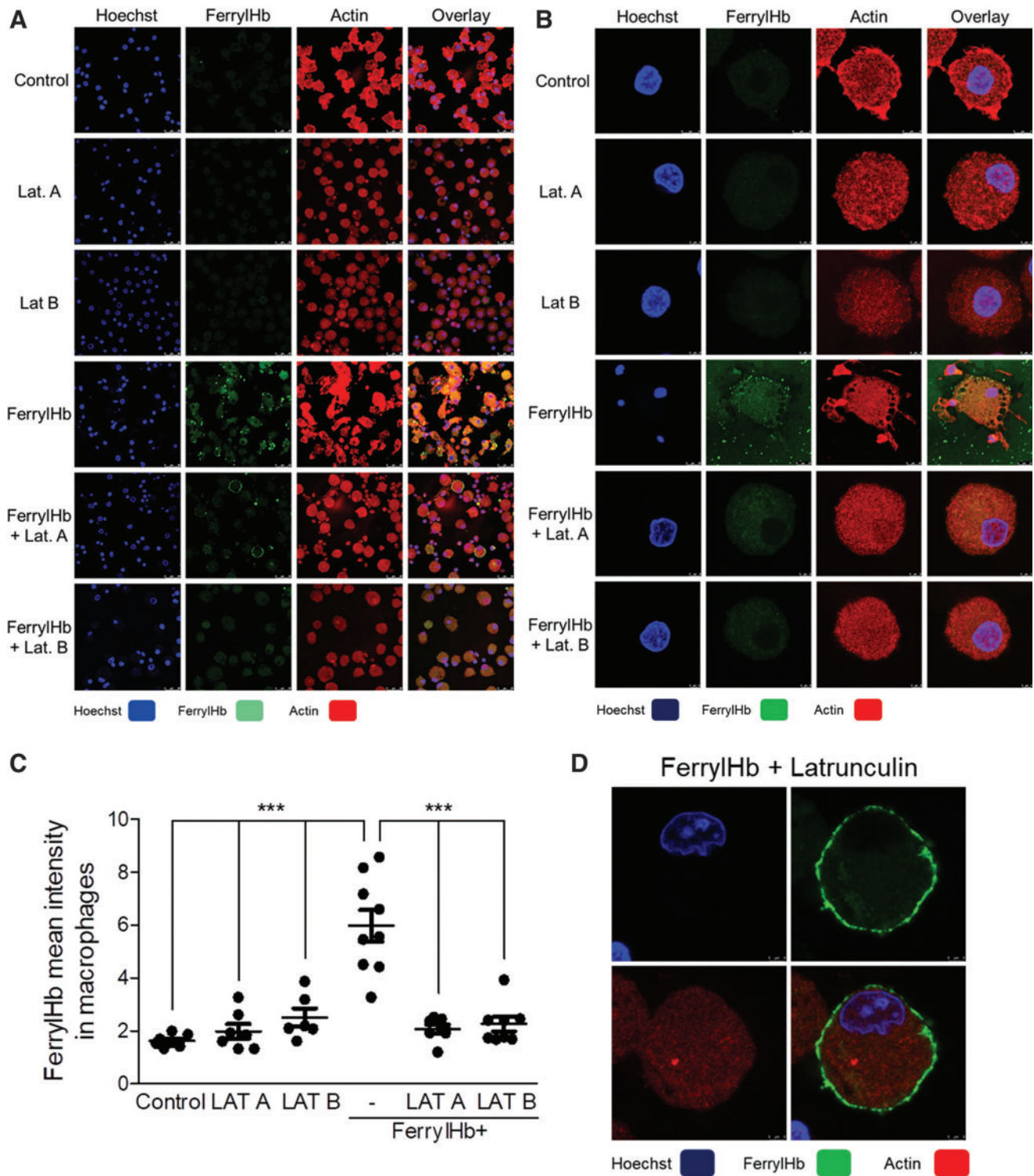
A

Hoechst | LAMP-1 | FerrylHb | F-actin | Merge

Control

oxyHb

FerrylHb

Hoechst ■ | LAMP-1 ■ | FerrylHb ■ | F-actin ■

B

Mean intensity of FerrylHb stainings

ns   ***

Control   oxyHb   FerrylHb

C

F-actin | FerrylHb

D

LAMP-1 | FerrylHb | Merge

LAMP-1 ■ | FerrylHb ■

E

LAMP-1   ← 120 kDa

Hb   } multimers

← 32 kDa
← 16 kDa

GAPDH   ← 37 kDa

Control FerrylHb

930

FIG. 8. **Inhibition of actin polymerization abrogates the uptake of ferryl hemoglobin by macrophages. (A, B, D)** Macrophages were grown on coverslips and then treated with LAT A (500 nM); LAT B (10 μM) in the presence or absence of ferrylHb (10 μM); or growth medium for 16 h. Cells were stained with Hoechst 33258 for DNA (*blue*), an anti-ferrylHb antibody with Alexa Fluor 488 secondary antibody for ferrylHb (*green*), and Ifluor746 for actin (*red*). **(A)** Low-magnification and **(B)** high-magnification of images were shown. Images were taken with Leica TCS SP8 gated STED-CW nanoscopy. Images were deconvolved using Huygens Professional software. **(C)** FerrylHb intensity of macrophages was calculated by ImageJ software. Scale bars shown in the images represent **(A, D)** 3 μm and **(B)** 25 μm. ***$p < 0.001$. LAT A, latrunculin A; LAT B, latrunculin B. Color images are available online.

dynamics simulations on Hb α,β dimeric form showed the Tyr36 radical of β chain, and its vicinity is far from the α chain. The formation of the Tyr36 radical of β chain was previously revealed by another research group using an off-line mass spectrometry method that combines immunospin trapping and chromatographic procedures (Supplementary Fig. S2) (56).

Immunohistochemical analysis using our new anti-ferrylHb antibody revealed that ferrylHb is localized extracellularly and also internalized by selected cell types, and the majority of ferrylHb-positive cells presented with morphological and immunophenotypic (CD68^{+}, lysozyme^{+}) features of macrophages in the human hemorrhagic transformation lesion (Fig. 4). We found that these macrophages were also expressing several proinflammatory molecules, including IL-1β and TNF-α (Figs. 2 and 6).

Monocyte-derived activated cells play a central role in the pathogenesis of atherosclerosis. The primary function of macrophages is to remove dead cells, pathogens, and debris by phagocytosis (24, 34, 50). To mimic the behavior of macrophages upon exposure to ferrylHb in atherosclerotic plaque, we exposed human macrophages to ferrylHb in cell culture. We observed that macrophages engulfed the ferrylHb in actin-lined phagocytic cups at the end of long thin pseudopodia within 12 h of exposure (Fig. 7). We detected uptake and transport of the ferrylHb to lysosomes in the macrophages (Fig. 7).

CD163 is a receptor for endocytosis of Hb-haptoglobin complexes in macrophages (23). Schaer *et al.* demonstrated that Hb interacts with CD163 in the absence of haptoglobin. Hb is internalized into an endosomal compartment by CD163 as a result of active receptor-dependent endocytosis. It was shown that Hb uptake also occurs after modifications such as $\alpha\alpha$-DBBF crosslinking or Hb polymerization (61, 62). The uptake of site-specific multiple peptide conjugate attached to βCys93 was demonstrated to be as efficient as the uptake of Hb-haptoglobin complex (62). Drawing on these observations, we hypothesized that the CD163 might represent a receptor for ferrylHb uptake, resulting in receptor-mediated endocytosis.

Using confocal microscopy and STED nanoscopy, we observed colocalization of ferrylHb with CD163 in macrophages of the human hemorrhagic atherosclerotic lesion. As we exposed macrophages to ferrylHb in culture, the same colocalization was found with CD163. Importantly, silencing the *CD163* gene decreased ferrylHb uptake providing direct evidence that internalization occurs *via* CD163 (Fig. 12). Therefore, we concluded that two ways exist to remove extracellular ferrylHb by macrophages.

Both phagocytosis and receptor-mediated endocytosis require actin polymerization (2, 38). In our experiments, inhibition of actin polymerization significantly inhibited ferrylHb uptake (Fig. 8). Further studies are needed to explore the mechanism of rearrangements in the actin cytoskeleton that lead to the internalization of ferrylHb.
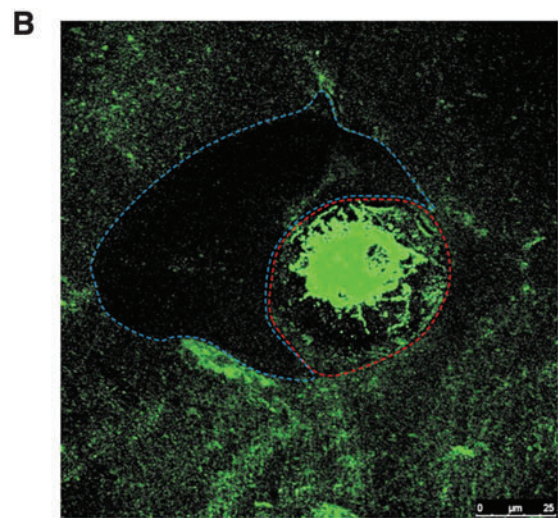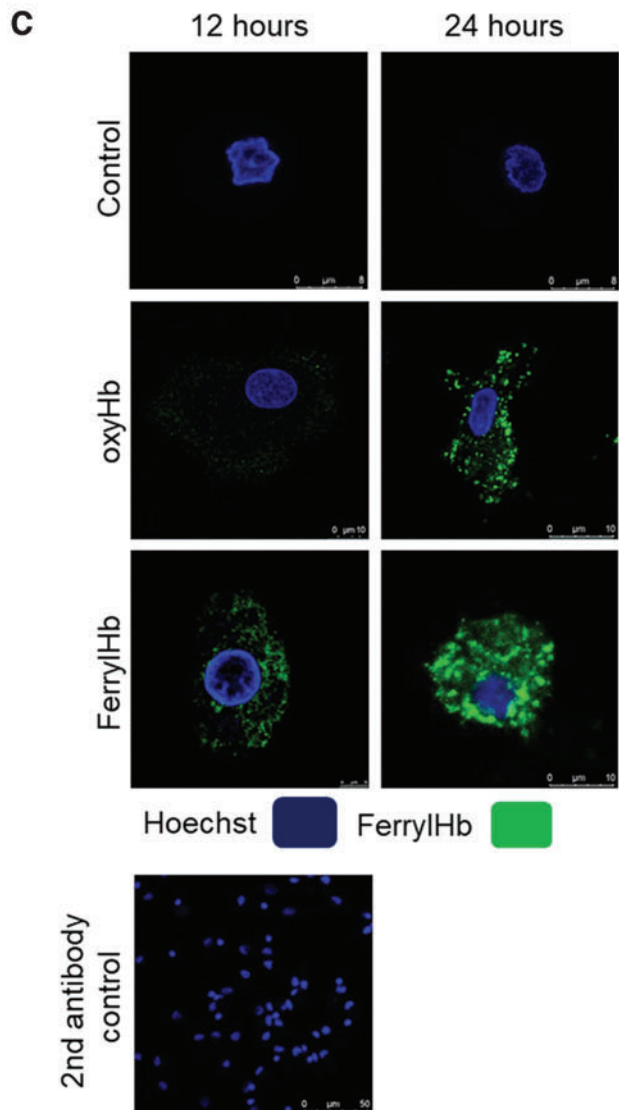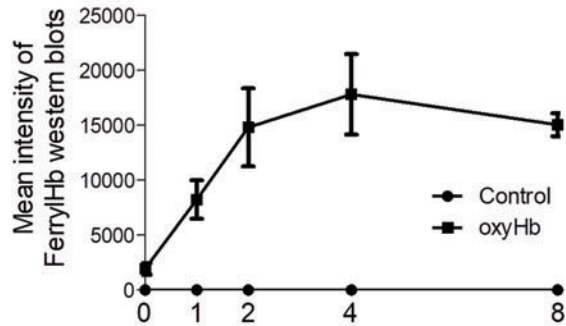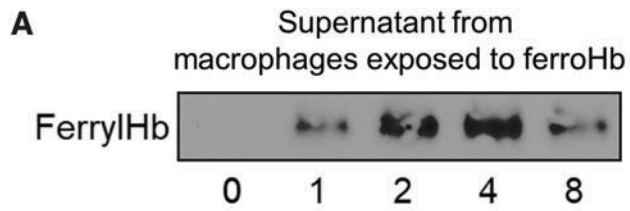
Since macrophages internalizing ferrylHb were found to express proinflammatory molecules, including IL-1β and TNF-α, in the human hemorrhagic atherosclerotic lesion (Fig. 6), we performed gene expression analyses using RNA-seq in macrophages exposed to ferrylHb. We observed that ferrylHb activates proinflammatory programs in macrophages by inducing the expression of inflammatory cytokines such as IL-1β, TNF-α, and CXCL8 and by decreasing the expression of anti-inflammatory cytokines such as CD209 and IL27RA (Fig. 13). This transcriptional program is unique and distinct from that of native Hb and significantly overlaps with gene expression changes in the complicated lesion (Fig. 15 and Supplementary Fig. S13). We demonstrated that proinflammatory gene expressions induced by ferrylHb in macrophages were driven by the activation of PI3K/HIF-1α/VEGF pathway (Fig. 14). These data suggest that ferrylHb represents a potent proinflammatory stimulus in the complicated atherosclerotic lesion.

Other pieces of evidence also suggest that ferrylHb possesses specific immunomodulatory activities acting on the vascular endothelium. Endothelium exposed to ferrylHb upregulates the expression of adhesion molecules (ICAM-1, VCAM-1, E-selectin) (67). Moreover, ECs treated with ferrylHb exhibit rearrangement of the actin cytoskeleton resulting in disruption of the EC monolayer, intercellular gap formation, and increased permeability of the monolayer (55, 67). In addition, ferrylHb was shown to induce inflammation in mice, and it is chemotactic for neutrophils when injected into the peritoneal cavity (67).
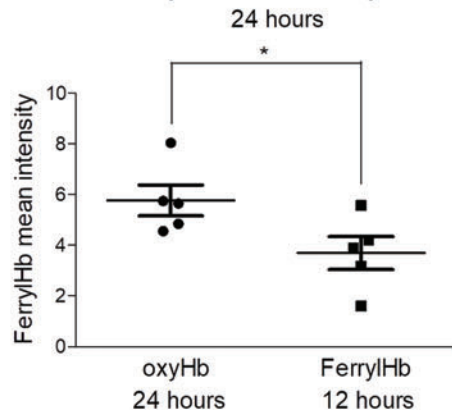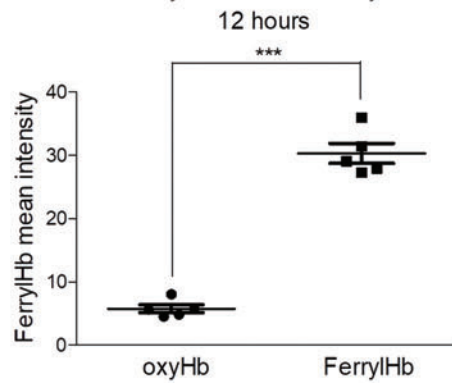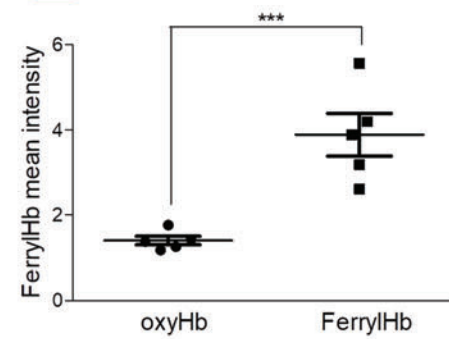
High expression of CD163 on macrophages was shown to be accompanied by reduced expression of proinflammatory cytokines such as TNF-α in humans (21). Although CD163^{+} macrophages are considered to have anti-inflammatory (1, 61) and atheroprotective (21) properties, Guo *et al.* recently showed that these macrophages exposed to oxyHb promote accelerated plaque angiogenesis, leakiness, inflammation, and progression *via* the CD163/HIF-1α/VEGF-A pathway in animal models of atherosclerosis (25).

It was demonstrated that internalization and transportation of native Hb to endosome with the CD163 scavenger receptor result in decreased cell surface expression of CD163 (61). Moreover, shedding of CD163 by ADAM17 also reduces CD163 content (20). Importantly, it was found that CD163

FIG. 9. Oxidation of hemoglobin by macrophages. (A) Macrophages were grown on coverslips and were exposed to oxyHb (10 μM). The supernatant of macrophages was removed after 1, 2, 4, and 8 h. FerrylHb content of supernatants was analyzed with Western blot. **(B)** Macrophages were grown on coverslips and were exposed to oxyHb (10 μM) for 24 h. Cells were stained with an anti-ferrylHb antibody with Alexa Fluor 488 secondary antibody for ferrylHb (*green*). Images were taken with Leica TCS SP8 gated STED-CW nanoscopy. Images were deconvolved using Huygens Professional software. **(C)** Macrophages were grown on coverslips and were exposed to oxyHb (10 μM) or ferrylHb (10 μM) for 12 and 24 h. Cells were stained with Hoechst 33258 for DNA (*blue*), an anti-ferrylHb antibody with Alexa Fluor 488 secondary antibody for ferrylHb (*green*). Images were taken with Leica TCS SP8 gated STED-CW nanoscopy. Images were deconvolved using Huygens Professional software. FerrylHb intensity of macrophages was calculated by ImageJ software. Scale bars shown in the images represent 8, 10 μm, and **(B)** 25 μm. *$p < 0.05$; ***$p < 0.001$. Color images are available online.

A Supernatant from macrophages exposed to ferroHb

FerrylHb

0   1   2   4   8

B

- - - FerrylHb engulfed area
- - - Macrophage
■ FerrylHb

C

	12 hours	24 hours
Control		
oxyHb		
FerrylHb		

Hoechst ■   FerrylHb ■

2nd antibody control

12 hours

24 hours

933

recycling and shedding enhance the expression of CD163 (72, 73). Our results are in accordance with these studies as the exposure of macrophages to ferrylHb led to a significant elevation of CD163 at both mRNA and protein levels, and that was accompanied by actin-mediated phagocytosis (Fig. 11).

To find further signatures for the impact of ferrylHb in atherosclerosis, we performed RNA-seq analysis on biopsies from patients who underwent endarterectomies. Distinct transcriptomic signatures of human carotid arteries in patients with atheromatic and complicated hemorrhage RNA-seq analysis demonstrated that human complicated lesions and atheromatous plaques have distinct transcriptomic profiles. Importantly, affected genes are primarily associated with macrophage and neutrophil activation, angiogenesis, and iron ion transport. Pathways specifically affected in complicated lesions include gene changes associated with PI3K signaling, lipid transport, tissue remodeling, and artery development. Targeted analysis of gene expression associated with calcification, apoptosis, and hemolytic-specific clusters indicates the increase in severity of complicated lesions compared with atheromatous lesions. Interestingly, several inflammatory gene sets, including interleukins and TLRs, as well as genes associated with iron metabolism, were also affected. These data demonstrate that complicated lesions can be distinguished from atheromatous lesions at the transcriptomic level, and the magnitude of inflammatory and iron metabolism pathway activation likely accounts for the drastic phenotype changes (Figs. 15 and 16).

The pathophysiologic role of ferrylHb is supported by transcriptional changes observed in patients with complicated lesions, and remarkably, these changes show a large degree of overlap to genes induced by exposure of macrophages to ferrylHb. Comparing the differential gene expression profiles in human macrophages exposed to ferrylHb and the complicated lesion profiles, an ~35% overlap was noted. Among these 462 genes, we found several inflammatory and iron metabolism gene clusters that are commonly regulated both in macrophages treated with ferrylHb and in hemorrhaged patients' samples (Fig. 16).
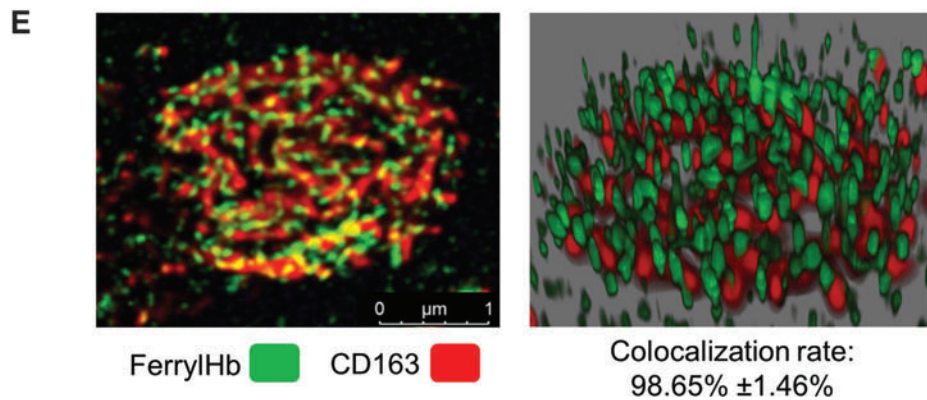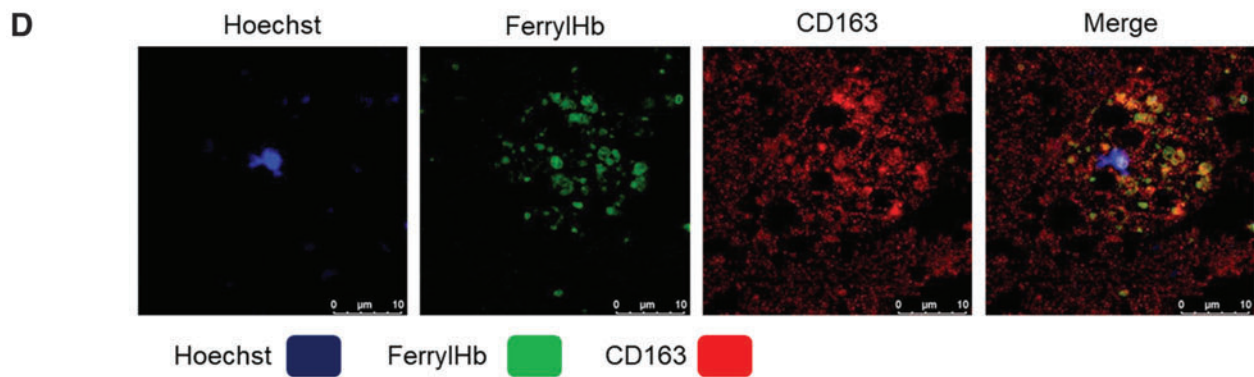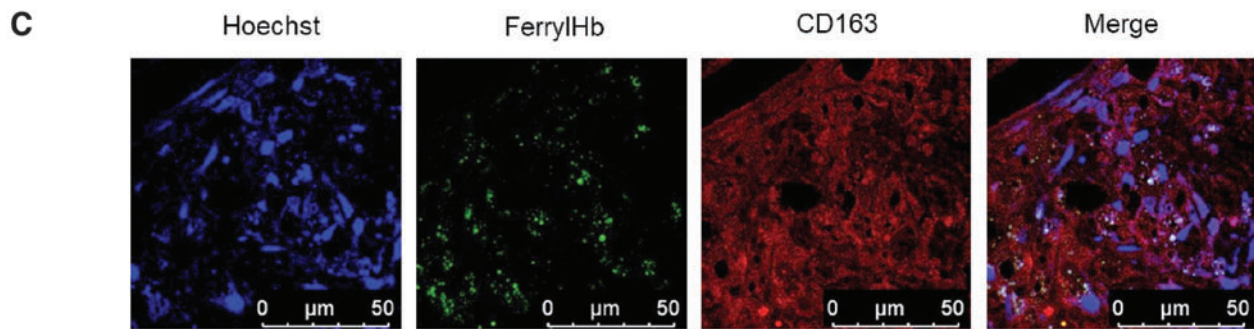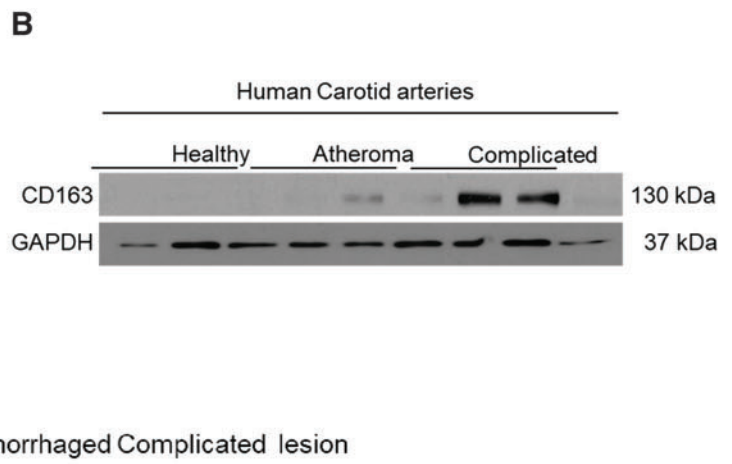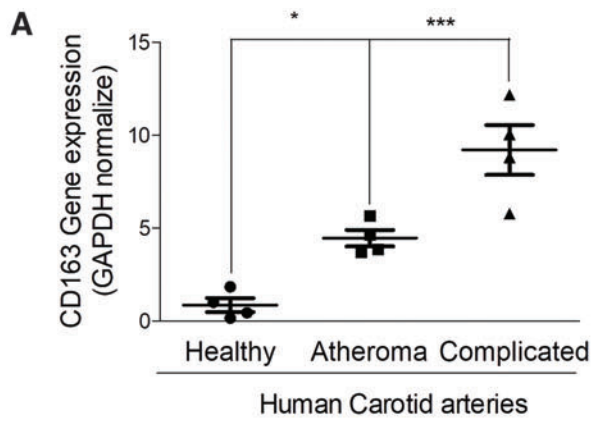
We summarize some future research directions and acknowledge some caveats. (i) In our study, we found an enhanced expression of H-ferritin without accumulation of iron in atheroma. Expression of H-ferritin is strongly regulated at the translational level by iron *via* the iron regulatory element/iron regulatory protein machinery. This involves the iron-dependent change in activity of the iron regulatory proteins 1 and 2 (60). Torti *et al.* previously revealed that inflammatory cytokines upregulate the expression of H-ferritin in the absence of iron (71). Since inflammation is the hallmark in the progression of atherosclerosis (66), the enhanced expression of H-ferritin can be explained by the elevation of inflammatory markers in atheroma. (ii) Both metHb and ferrylHb are able to release heme moieties, and thereby increase the expression of HO-1 in various cell types. It was previously demonstrated that metHb loses heme more readily than ferrylHb (36). To our surprise, induction of HO-1 by ferrylHb in macrophages was more pronounced than in cells exposed to metHb (Supplementary Fig. S8). This might be explained by the fact that ferrylHb is taken up by macrophages, and therefore, the induction is dependent not only upon heme release. (iii) The induction of HO-1 was significantly lower in macrophages after oxyHb treatment compared with cells exposed to ferrylHb (Supplementary Fig. S8). Our results on the expression of HO-1 in macrophages exposed to oxyHb and ferrylHb are in accordance with previous studies (36, 55). (iv) A very important area is to study the pathophysiologic role of apoptotic RBCs containing Hb in the progression of atherosclerosis (63). This is emphasized by the finding that oxidation of Hb also occurs in RBCs exposed to plaque material (Supplementary Fig. S4). (v) Alteration of transcriptomic profiles of atherosclerotic lesions depends upon not only the polarization of cells including macrophages but the change in cellular composition of atherosclerotic plaques as well. Future studies are needed to clarify the contribution of various cell types to the distinct transcriptomic profiles and to explore the exact signalization responsible for such cellular responses to ferrylHb.

Summary Graphic Illustration

Oxidized Hb commonly accumulates in atherosclerotic lesions as a result of RBC infiltration and lysis. FerrylHb generated by Hb oxidation in hemorrhagic transformed plaques is internalized *via* phagocytosis and CD163 receptor-mediated endocytosis independently from haptoglobin and then transported into lysosomes. Internalization of ferrylHb is accompanied by upregulation of HO-1 and H-ferritin and accumulation of iron within lysosomes as a result of heme/iron uptake. Polarization of macrophages induced by ferrylHb results in a distinct transcriptomic profile affecting gene expressions associated with inflammation, angiogenesis, tissue remodeling, iron metabolism, apoptosis, PI3K signaling, lipid transport, and calcification, thereby contributing to the transformation of atherosclerotic lesions toward a proatherogenic phenotype.

FIG. 10. Ferryl hemoglobin is colocalized with CD163 receptor in hemorrhagic transformed lesions. (A) Healthy ($N=4$), atheromatous ($N=4$), and hemorrhagic transformed ($N=4$) vessel relative expressions of CD163 were analyzed by real-time qPCR. **(B)** Healthy ($N=3$), atheromatous ($N=3$), and hemorrhagic transformed ($N=3$) vessel protein expressions of CD163 were analyzed by Western blot. **(C)** Segmental cross sections of a carotid artery demonstrating hemorrhagic transformed lesions were shown using immunofluorescent staining. **(D)** High-magnification images demonstrated ferrylHb and CD163-positive macrophage in the hemorrhagic transformed lesions. Sections were stained with Hoechst 33258 for DNA (*blue*), an anti-ferrylHb antibody with Alexa Flour 488 secondary antibody for ferrylHb (*green*), and anti-CD163 antibody with Alexa Flour 647 secondary antibody for CD163 (*red*). Images were taken with Leica TCS SP8 gated STED-CW nanoscopy. Images were deconvolved using Huygens Professional software. **(E)** Super-resolution images (2D and 3D technics) confirmed the colocalization of ferrylHb and CD163 receptor. Representative image, $n=5$. *$p<0.05$; ***$p<0.001$. Scale bars shown in the images represent 1, 10, or 50 μm. 2D, two dimensional; 3D, three dimensional; qPCR, quantitative polymerase chain reaction. Color images are available online.
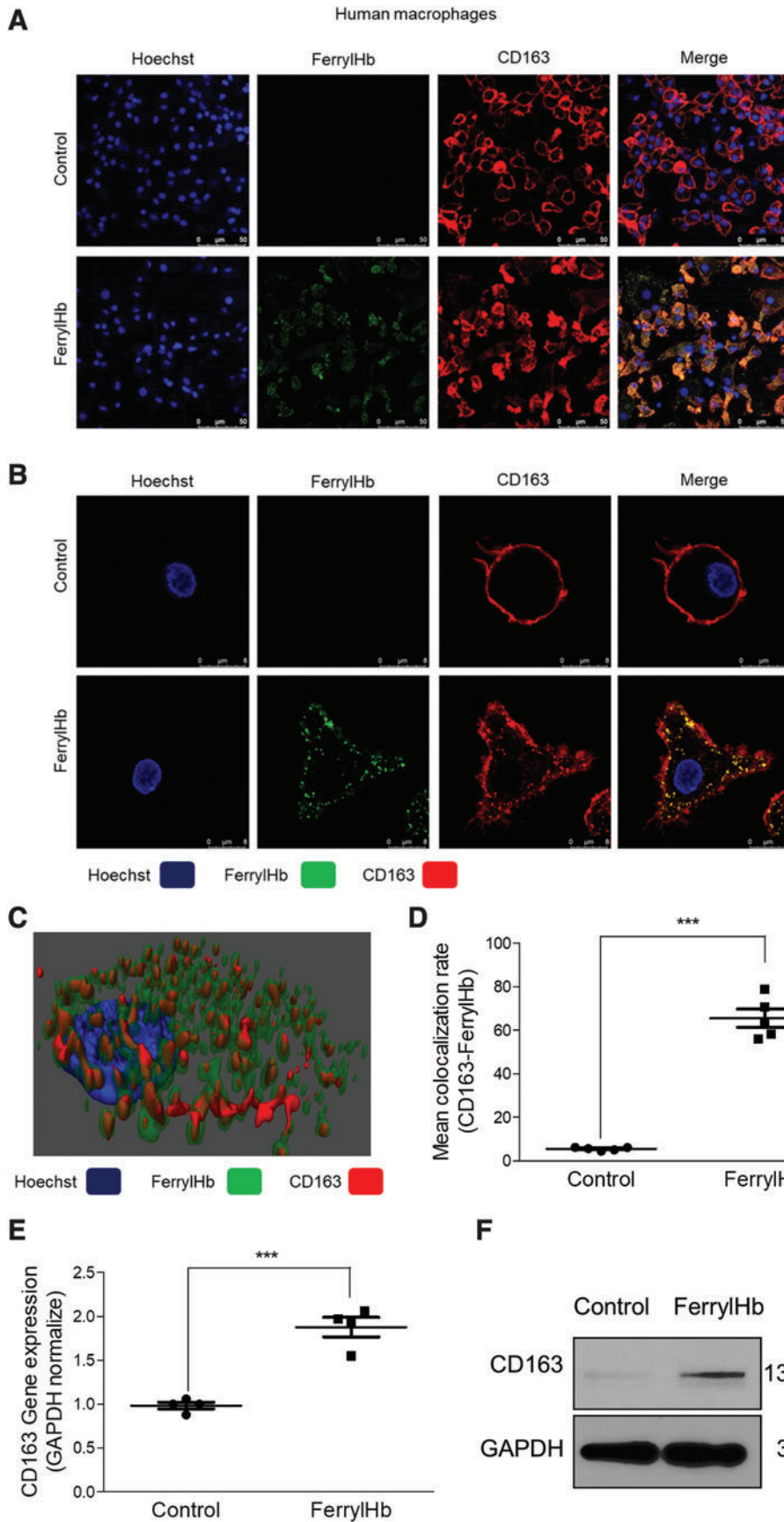
A CD163 Gene expression (GAPDH normalize)

Human Carotid arteries

B Human Carotid arteries

Healthy   Atheroma   Complicated

CD163   130 kDa

GAPDH   37 kDa

Human hemorrhaged Complicated lesion

C   Hoechst   FerrylHb   CD163   Merge

0 μm 50   0 μm 50   0 μm 50   0 μm 50

D   Hoechst   FerrylHb   CD163   Merge

0 μm 10   0 μm 10   0 μm 10   0 μm 10

Hoechst   FerrylHb   CD163

E

0 μm 1

FerrylHb   CD163

Colocalization rate:
98.65% ±1.46%

FIG. 11. Ferryl hemoglobin and CD163 receptor are colocalized in macrophages exposed to ferryl hemoglobin. (A, B) Macrophages grown on coverslips were exposed to ferrylHb ($10\,\mu M$) or growth medium for 16 h. Cells were stained with Hoechst 33258 for DNA (*blue*), an anti-ferrylHb antibody with Alexa Fluor 488 secondary antibody for ferrylHb (*green*), and an anti-CD163 antibody with Alexa Flour 647 secondary antibody for CD163 receptor (*red*). Images were taken with Leica TCS SP8 gated STED-CW nanoscopy. Images were deconvolved using Huygens Professional software. Representative image, $n=5$. (C) 3D image demonstrated colocalization of ferrylHb and CD163 receptor. (D) The colocalization rate of ferrylHb and CD163 was calculated by ImageJ software ($n=5$). (E) Macrophages were exposed to ferrylHb ($10\,\mu M$) or growth medium for 16 h. Relative expression of CD163 in cells was analyzed by real-time qPCR ($n=5$). (F) Macrophages were exposed to ferrylHb ($10\,\mu M$) or growth medium for 16 h. The expression of CD163 was assessed by Western blot ($n=4$). Scale bars shown in the images represent 25 or 50 μm. ***$p<0.001$. Color images are available online.
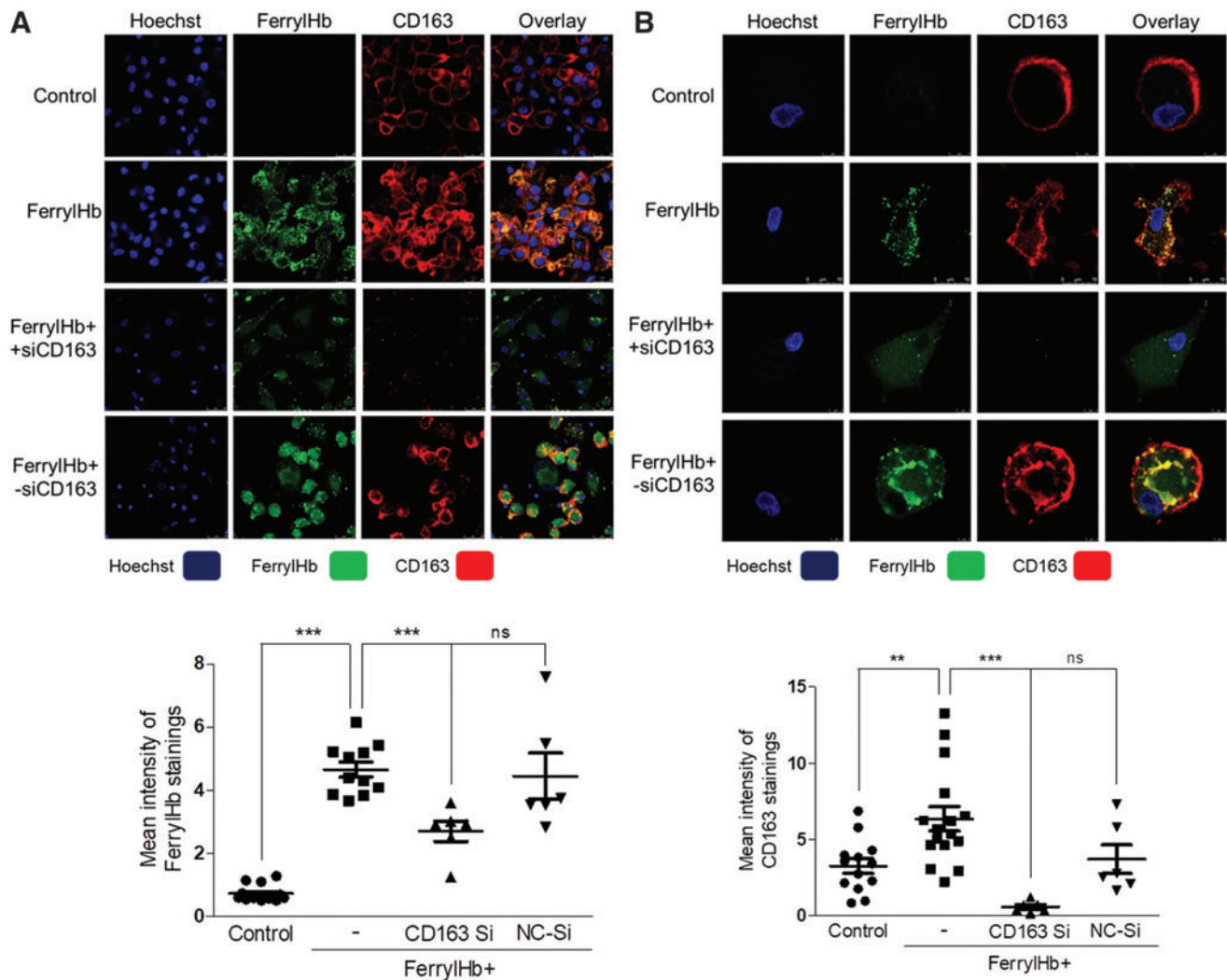
FIG. 12. Internalization of ferryl hemoglobin *via* CD163 receptor. (A, B) Macrophages were grown on coverslips and were exposed to ferrylHb (10 μM; *second row*) in the presence or absence of siRNA against CD163 receptor (200 nM; *third row*) or with—siRNA (200 nM; *fourth row*) for 16 h. Cells were stained with Hoechst 33258 for DNA (*blue*), an anti-ferrylHb antibody with Alexa Fluor 488 secondary antibody for ferrylHb (*green*), and an anti-CD163 antibody with Alexa Fluor 647 antibody for CD163 (*red*). **(A)** Low-magnification and **(B)** high-magnification images were shown. Images were taken with Leica TCS SP8 gated STED-CW nanoscopy. Images were deconvolved using Huygens Professional software. **(A,** *lower panel*) FerrylHb intensity of macrophages was calculated by ImageJ software. **(B,** *lower panel*) CD163 intensity of macrophages was calculated by ImageJ software. Scale bars shown in the images represent **(B)** 5 μm and **(A)** 25 μm. *******p* < 0.01; ********p* < 0.001. siRNA, small interfering RNA. Color images are available online.

Methods (Electronic Laboratory Notebook Was Not Used)

All reagents were purchased from Sigma-Aldrich (Darmstadt, Germany) with ACS grade or higher purity except when otherwise specified below.

Study approval and collection of carotid artery samples

Carotid arteries from patients who underwent carotid endarterectomies were obtained from the department of surgery. Samples were collected from 135 patients between October 2012 and January 2021. The eligible cases represented 11.5% of the total surgical interventions (1170) performed for carotid endarterectomy in the study period (Table 1). We excluded samples of human carotid arteries

that did not meet the following criteria: (i) were not received within 1 h after surgical interventions, (ii) RNA and protein degradation occurred, (iii) blood clot in the artery, and (iv) not an appropriate collection of samples. Ninety-seven complicated lesions, 25 atheromatous plaques, and 13 healthy samples were used for spectrophotometric analysis, proteomic analysis, biochemical examination, molecular biology studies, immunohistochemistry, and RNA-sequencing. Figure legends of experiments include the number of samples used (Figs. 1–6, Fig. 10 and Figs. 15, 16). The collection of carotid arteries was approved by the Scientific and Research Ethics Committee of the Scientific Council of Health of the Hungarian Government under the registration number of DE OEC RKEB/IKEB 3712-2012 (September 25, 2012). Written informed consent was received from the participants. Healthy
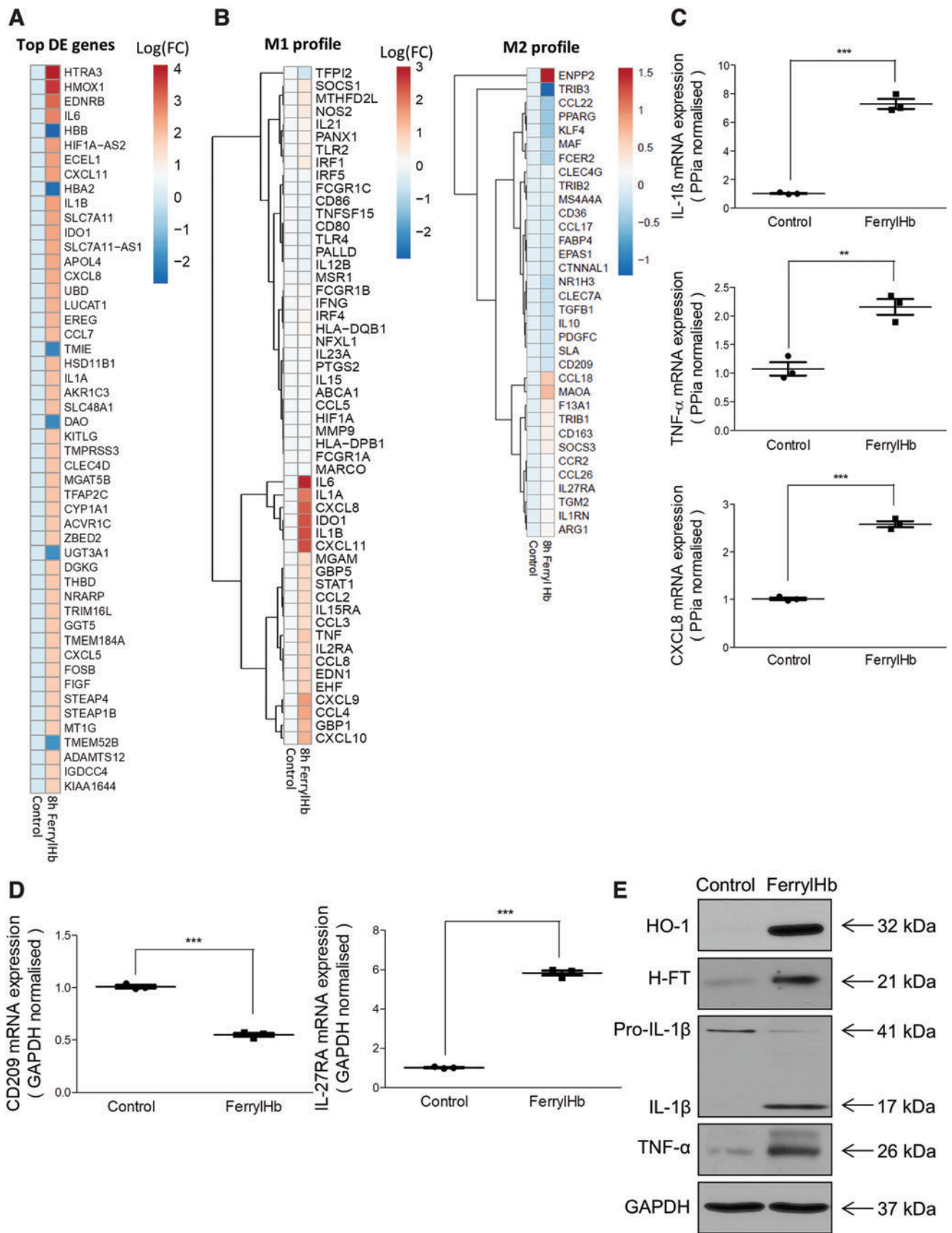
FIG. 13. **Transcriptomic analysis reveals that ferryl hemoglobin polarizes macrophages into a proinflammatory-like phenotype.** **(A, B)** RNA-seq transcriptomic analysis was performed on human macrophages treated with ferrylHb (10 μM) for 8 h ($n = 4$/group). **(A)** Heatmap of the 50 most-changed DE genes is shown in $\log_{10}$(FC). **(B)** M1 and M2 signatures are shown as a clustered heatmap in $\log_{10}$(FC). **(C, D)** Relative expression of **(C)** IL-1β, TNF-α, CXCL8, **(D)** CD209, and IL-27RA were analyzed by real-time qPCR ($n = 3$). **(E)** Protein expression of HO-1, H-ferritin, Pro-IL-1β, IL-1β, TNF-α and GAPDH was determined by Western blots in macrophages exposed to ferrylHb (10 μM, 8-h ferrylHb treatment). ******$p < 0.01$; *******$p < 0.001$. DE, differentially expressed; FC, fold change. Color images are available online.
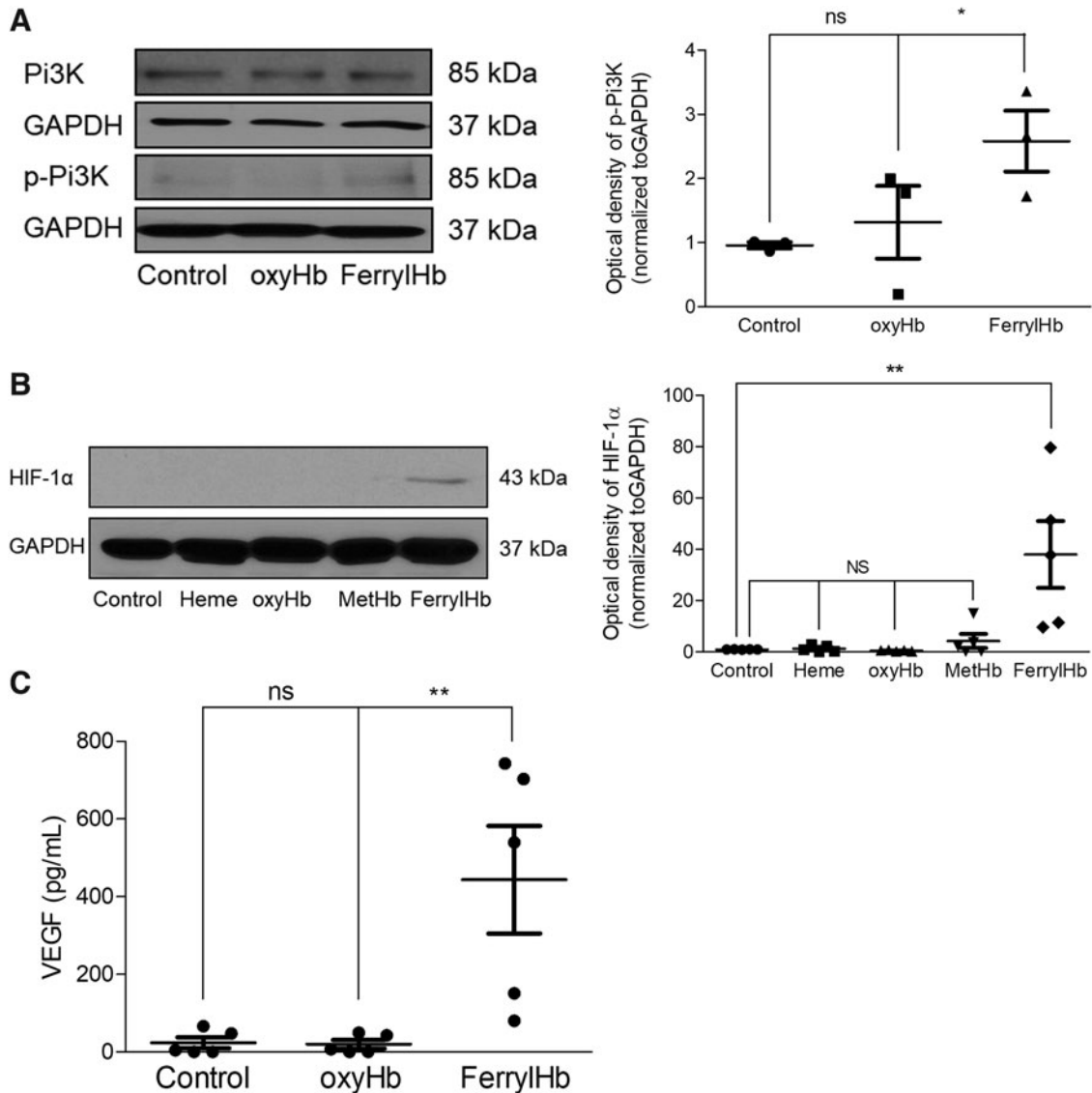
FIG. 14. PI3K/HIF-1α/VEGF pathway in macrophages exposed to ferryl hemoglobin. (A) Human macrophages were treated with 10 μM oxyHb or ferrylHb for 2 h. The expression of PI3K and phopsho-PI3K protein was assessed by Western blot ($n=3$). **(B)** Human macrophages were treated with 10 μM heme, oxyHb, metHb, or ferrylHb for 16 h. The expression of HIF-1α was assessed by Western blot ($n=5$). **(C)** Human macrophages were treated with 10 μM oxyHb or ferrylHb for 24 h. The secreted VEGF-A was measured by the ELISA-kit. $*p<0.5$; $**p<0.01$. ELISA, enzyme-linked immunosorbent assay; HIF-1α, hypoxia-inducible factor 1-alpha; PI3K, phosphoinositide 3-kinase; VEGF, vascular endothelial growth factor.

FIG. 15. Transcriptomic analysis of human carotid arteries. (A) RNA-seq transcriptomic analysis was performed on human carotid arteries from atheromatous (Patient number = 5, *yellow circle*) and complicated (Patient number = 4, *blue circle*) lesions, as well as those from healthy carotid arteries ($N=4$, *black rectangle*). PCA plot shows the variance from these three groups. Unit variance scaling is applied to *rows*; SVD with imputation is used to calculate principal components. *X* and *Y* axes show principal component 1 and principal component 2, explaining 22.5% and 20.3% of the total variance, respectively. **(B)** Scatter plot depicting the number of DE genes of each group comparison. *Y*-axis shows the DE genes in the complicated lesion *versus* healthy sample (6408 genes) and *X*-axis the atheromatous *versus* healthy comparison (4237 genes). Data sets were filtered for logFC >2 and top genes passing these criteria are labeled. **(C, D)** Targeted clustered analysis showing absolute expression patterns of genes associated with **(C)** calcification, apoptosis, and hemolysis, as well as **(D)** iron metabolism and inflammation from healthy, atheromatous, and complicated lesion groups. Gene expression levels were calculated using DESeq and are displayed as a normalized expression [=log(raw counts)]. PCA, principal component analysis; SVD, singular value decomposition. Color images are available online.
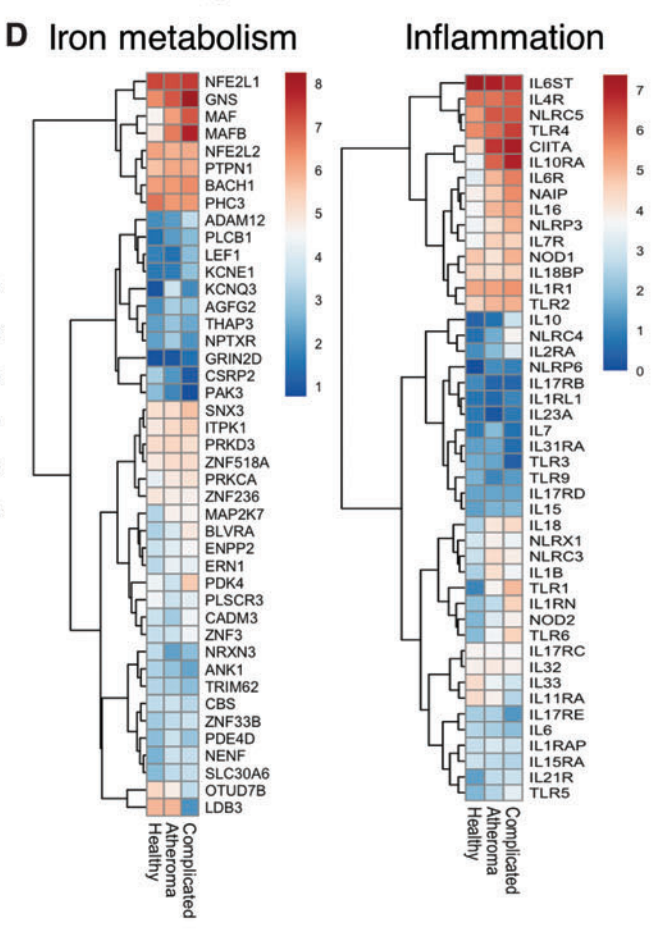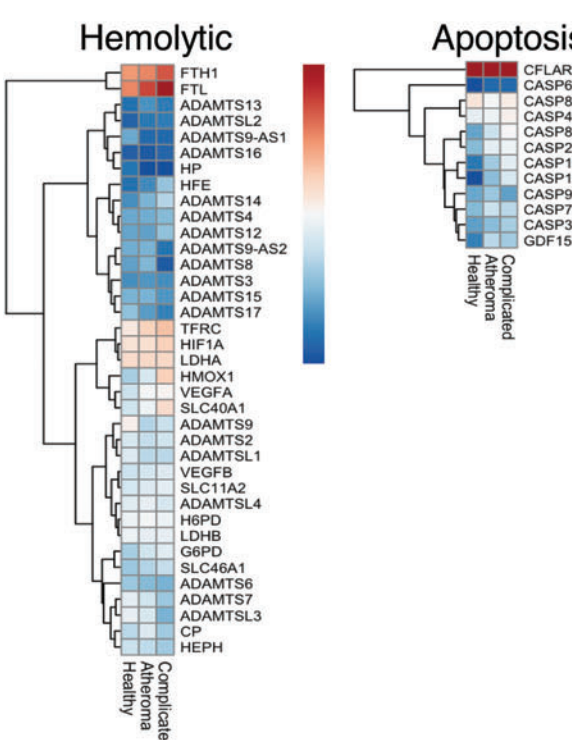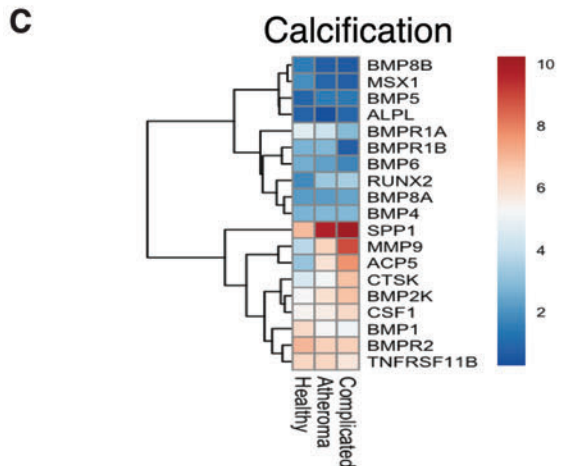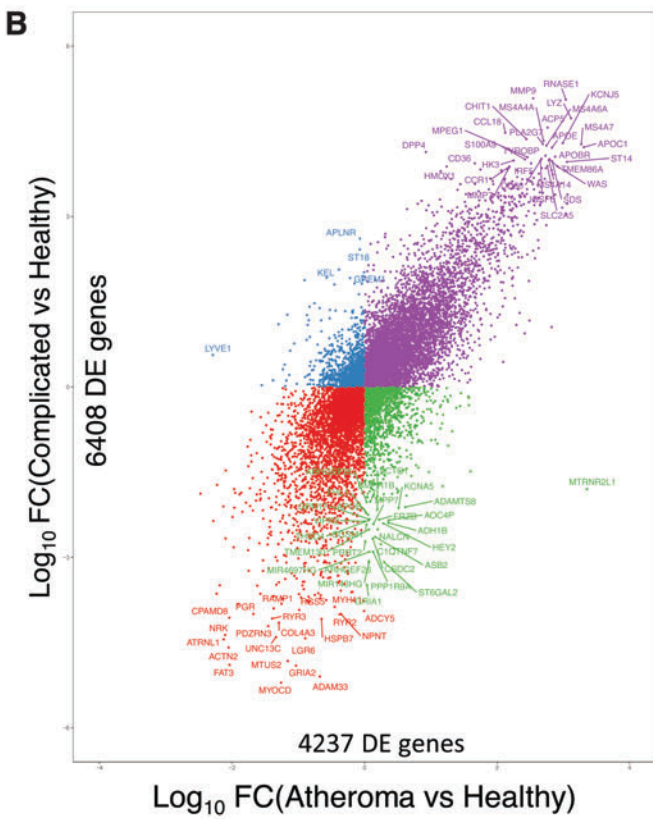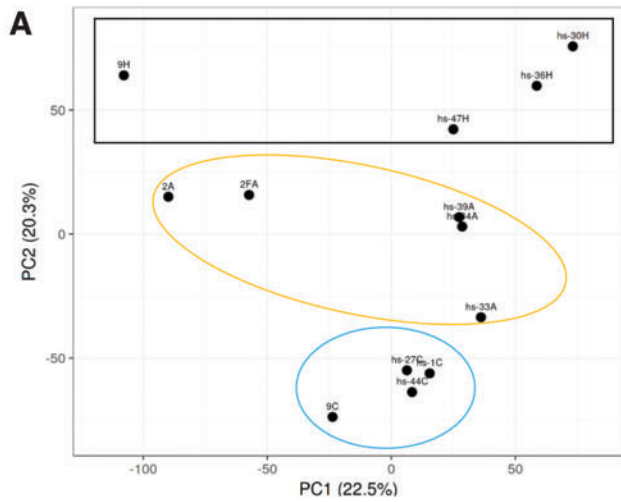
carotid arteries for controls were obtained from cadavers ($N = 13$) of suicide or traumatic events without cardiovascular diseases from the department of forensic medicine (Regional Research Ethical Committee, Project No. 5038-2018). A pathologist examined the specimens and classified them according to AHA guidelines (69). Type IV (atheromatous) and type VI (complicated) lesions, as well as healthy carotid arteries, were selected for further investigation. Histological characterization was performed for all carotid artery samples. The numbers of tissue samples used for each experiment were added to Figure legends (Figs. 1–6, Fig. 10 and Figs. 15, 16). Macrophages from healthy volunteers were isolated from whole blood (Regional Research Ethics Committee, Project No. 3853-2013 and 4699-2016).
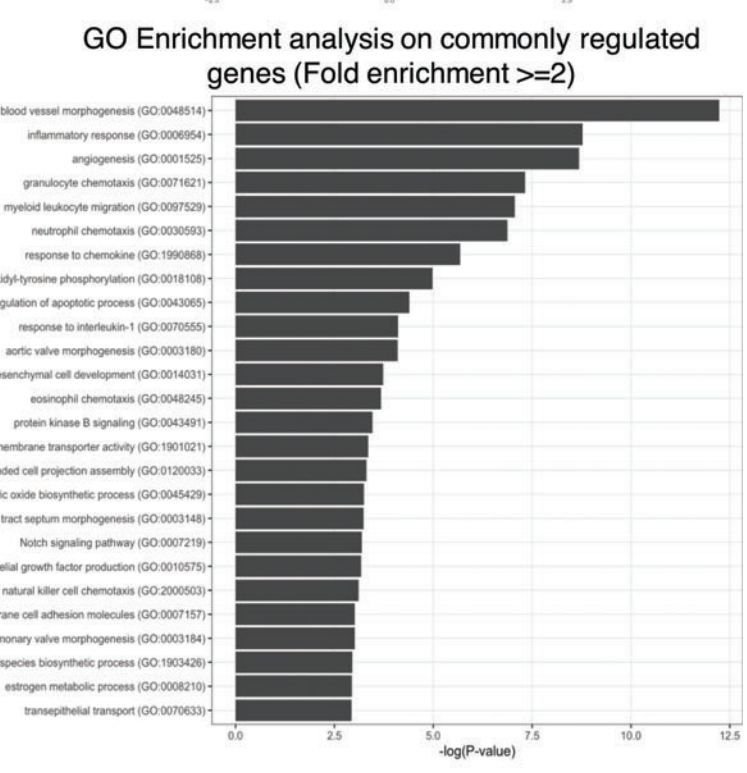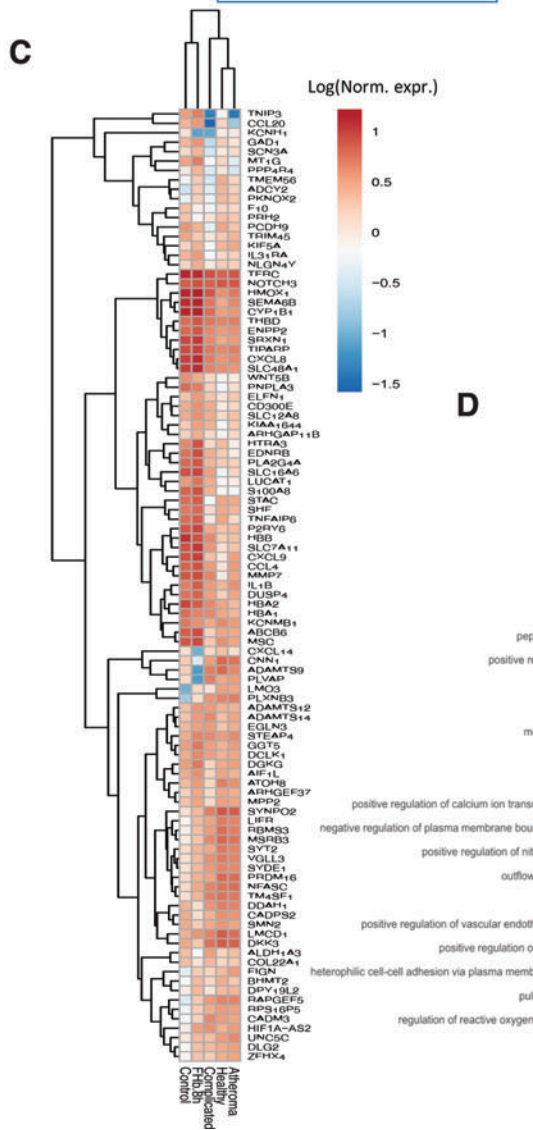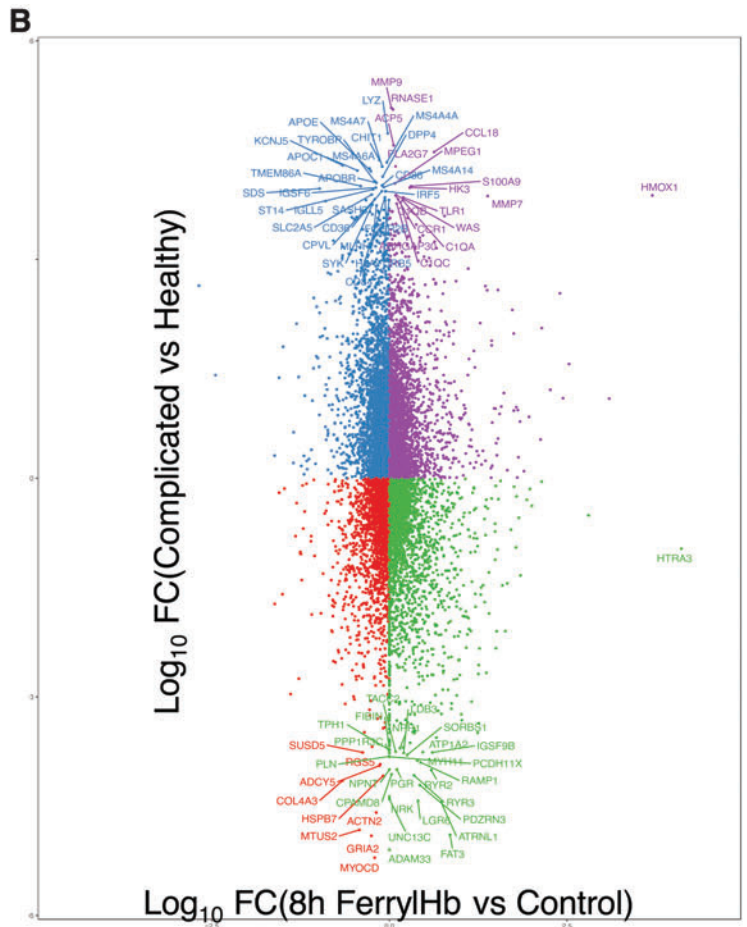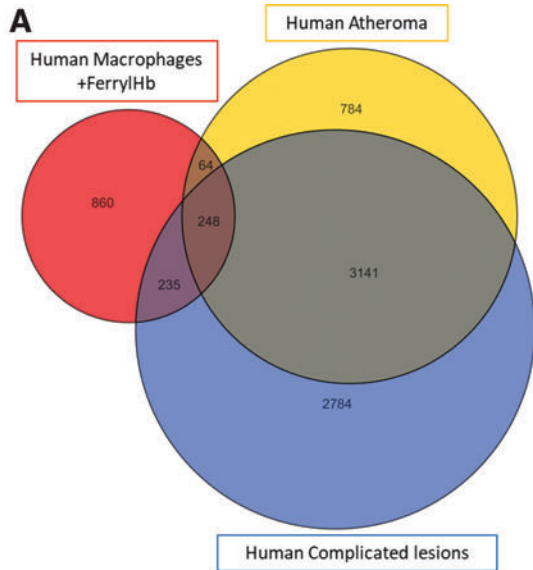
Histology

Tissue sections of 4 μm thickness from representative formalin-fixed paraffin-embedded tissues were used for serial H&E and special and immunohistochemical stainings. Deparaffination, antigen retrieval, staining for CD68, glycophorin A, carboxypeptidase M, HMOX1, ferritin heavy chain, TNF-α, IL-1 β, and ferrylHb antibody were performed according to the instructions of the manufacturer with CD68 antibody (Roche Mo. Kft, KP-1 clone) without dilution (ready to use) for 1 h; with the glycophorin A antibody (M081901-2, clone: JC159; Dako, an Agilent Technologies Company) at a dilution of 1:1000 for 1 h; with the carboxypeptidase M antibody (ab150405 clone: EPR8052; Abcam Plc, Cambridge, United Kingdom) at a dilution of 1:200 for 1 h; with the HMOX1 antibody (10701-1-AP, polyclonal; Invitrogen) at a dilution of 1:400 for 1 h; with the ferritin heavy chain antibody (ab75972 clone: EPR3005Y; Abcam Plc) at a dilution of 1:50 for 1 h; with the IL-1 beta antibody (P420B, polyclonal ab; Invitrogen) at a dilution of 1:100 for 1 h; with the TNF-α antibody (PA5-19810, polyclonal ab; Invitrogen) at a dilution of 1:100 for 1 h, and with the mouse anti-human ferrylHb antibody (made by our groups) at a dilution of 1:100 for 1 h. Staining was performed in a Ventana BenchMark Ultra immunostainer (Roche Diagnostics) in the following circumstances: Antibody Diluent, Cat. No. 251-018 (contains 0.3% protein in 0.1 M phosphate-buffered saline [pH 7.3] and 0.05% ProClin 300, a preservative). Incubation time: 1 h. Epitope retrieval, HIER: on Machine. Buffer: ULTRA Cell Conditioning Solution (ULTRA CC1; contains: Tris-based buffer and a preservative) Heating time: 20–35 min. Maximum heating temperature: 95°C, Visualization system Producer: Ventana Product no: ultraView

Universal DAB (Cat. No. 760–500). For digital documentation, slides were scanned with the Mirax Midi scanner (3D Histech, Budapest, Hungary). Macroscopic pictures of the arteries were taken with a Nikon D3200 camera (Nikon Corp., Minato, Japan).

Western blot

Healthy arteries ($N = 9$), atheroma plaques ($N = 9$), and hemorrhaged plaques ($N = 9$) were homogenized in liquid nitrogen. Then, the samples were solubilized in protein lysis buffer (10 mM Tris-HCl, 5 mM EDTA, 150 mM NaCl (pH 7.2), 1% Triton X-100, 0.5% Nonidet P-40, and protease inhibitors (Complete Mini; F. Hoffmann-La Roche Ltd., Basel, Switzerland)). Twenty-microgram proteins of each sample were loaded on SDS-polyacrylamide (12.5%) gels. In another case, 500 ng purified Hb was adjusted into an SDS (12.5%) or native gel (6%). After electrophoresis, proteins were transferred to a nitrocellulose membrane (Amersham Biosciences Corp., Piscataway, NJ). The blot was incubated with HRP-conjugated goat anti-human Hb antibody (Cat. No. ab19362-1; Abcam Plc) at a dilution of 1:5000 for 2 h or with the mouse anti-human ferrylHb antibody labeled with HRP (developed by our groups) at a dilution of 1:1000 for 2 h or with the rabbit anti-human CD163 antibody (NB110-40686; Novusbio) at a dilution of 1:1000 overnight followed by the HRP-conjugated secondary antibody. The antigen/antibody complex was detected with chemiluminescence according to the manufacturer's instructions (GE Healthcare Life Sciences, Piscataway, NJ). Quantification of the signals was performed using ImageJ software. Human macrophages were treated with 10 μM ferrylHb for 8, 12, or 16 h. After treatment, the cells were solubilized in protein lysis buffer. Twenty micrograms of total protein was applied to 10% SDS-PAGE gels. Proteins were identified using the following antibodies: rabbit anti-human HO-1 antibody (10701-1-AP, dilution: 1:2500; Proteintech, Rosemont, IL), rabbit anti-human H-ferritin antibody (sc-25617, dilution: 1:500; Santa Cruz, Dallas, TX), rabbit anti-human IL-1β antibody (P420B, dilution: 1:500; Thermo Fisher, Rockford, IL,), rabbit anti-human TNF-α antibody (P300A, dilution: 1:500; Thermo Fisher), and rabbit anti-human CD163 antibody (NB110-40686; dilution: 1:1000; Novusbio). Human macrophages were treated with 10 μM ferrylHb for 24 h, followed by the cells solubilized in protein lysis buffer. Twenty micrograms of total protein was applied to 10% SDS-PAGE gels. The CD36 protein was incubated with the rabbit anti-human CD36 antibody (PA1-16813; dilution: 1:1000;

FIG. 16. Comparative analysis between atherosclerotic lesions and human macrophages exposed to ferryl hemoglobin. (A) Venn diagram depicting the number of DE genes by each group analyzed. *Blue circle* refers to the number of DE genes in complicated lesions *versus* healthy samples. *Orange circle* is associated with the number of DE genes in atheromatous lesions *versus* healthy samples and *red* refers to the number of DE genes in human macrophages treated with ferrylHb for 8 h. (B) Scatter plot depicting the number of commonly regulated genes from each group comparison. *Y*-axis shows the DE genes in the complicated lesion *versus* healthy sample, and *X*-axis the human macrophages treated with ferrylHb comparison. Data sets were filtered for logFC >2 and top genes are labeled. (C) Clustered heatmap analysis of genes belonging to the commonly regulated and overlapping gene set (547 genes) from the Venn diagram in Figure 12A. Gene expression levels are displayed as $\log_{10}$ (normalized expression). (D) GO pathway enrichment analysis on common overlapping DE genes in complicated and atheromatous lesions when compared with healthy donors, and human macrophages treated with ferrylHb compared with control. Top pathways are shown with at least twofold enrichment and ranked based on $-\log(p$ value). GO, Gene Ontology. Color images are available online.

A Human Macrophages +FerrylHb / Human Atheroma / Human Complicated lesions

B Log$_{10}$ FC(Complicated vs Healthy) vs Log$_{10}$ FC(8h FerrylHb vs Control)

C Log(Norm. expr.)

D GO Enrichment analysis on commonly regulated genes (Fold enrichment >=2)

942

Invitrogen) overnight followed by the HRP-conjugated rabbit secondary antibody (ab6721; Abcam Plc) at a dilution of 1:4000 for 2 h. Uncropped raw images of all blots were inserted as Supplementary Figures S14–S23.

Hb separation and purification

OxyHb (Fe^{2+}) and ferrylHb (Fe^{4+}) were prepared as described before (67). Hb was isolated from fresh blood drawn from healthy volunteers and purified using ion-exchange chromatography on a DEAE Sepharose CL-6B column. Isolation of Hb from RBCs yielded 98%–99% oxyHb, and 1%–2% of Hb undergoes oxidation. FerrylHb was generated by incubation of oxyHb with a 10:1 ratio of H_2O_2 for 5 h at 37°C. After the oxidation, Hb solutions were dialyzed against saline (three times for 1 h at 4°C) and concentrated with Amicon Ultracentrifuge filter tubes (10,000 MWCO; Millipore Corp., Billerica, MA). Aliquots were snap-frozen in liquid nitrogen and kept at −70°C. The purity of Hb preparation was assessed by silver staining. Hb concentrations were calculated as described by Winterbourn (75). In the present study, the Hb concentration was always expressed as heme concentration.

LDL isolation

LDL was isolated from the plasma of healthy volunteers with gradient ultracentrifugation (Beckman Coulter, Inc., Brea, CA). The density of plasma (1.3 g/mL) was adjusted with KBr, and a two-layer gradient was prepared in a Quick-Seal ultracentrifuge tube by layering saline on the plasma. Ultracentrifugation was done at 50,000 rpm for 2 h at 4°C (Type 50.2 Ti Rotor; Beckman Coulter, Inc.). LDL samples were kept at −70°C until use, and the protein concentration was measured by the Pierce BCA Protein Assay Kit (Pierce Biotechnology, Rockford, IL).

Isolation of plaque lipids

Lipids from the human carotid artery were extracted as described previously (9).

Oxidation of LDL and plaque lipids

For LDL oxidation, 200 μg/mL of LDL was incubated with 5 μM heme in the presence of 75 μM H_2O_2 for 1 h at 37°C. Oxidation of plaque lipids was carried out in a reaction mixture containing 0.5 mg/mL plaque lipids and 5 μM heme for overnight incubation at 37°C.

Oxidation of Hb

Five micromolars of purified Hb was incubated with 50 μM of H_2O_2, or 25 μM of LOOH (cumene hydroperoxide; an analogue of LOOH), or 100 μg/mL of oxLDL, or 500 μg/mL of oxPL for 2 h at 37°C.

Oxidation of RBCs

Whole peripheral venous blood was drawn from healthy volunteers, and RBCs were obtained by centrifugation (2000 g, 15 min, 4°C). The samples were immediately incubated with 75 μM LOOH or 500 μg/mL oxPL for 2 h at 37°C. After the incubation, samples were centrifugated (2000 g, 15 min, 4°C) and the supernatant was measured with a spectrophotometer (Beckman Coulter, Inc.). Next, the RBC pellet was

washed with saline and centrifugated (2000 g, 15 min, 4°C). Then the supernatant was discarded, and the pellet was lysed with destillated water. Finally, the supernatant was measured with a spectrophotometer (Beckman Coulter, Inc.). MetHb (Fe^{3+}) percent was calculated as described by Winterbourn (75). Twenty microliters of lysed RBC was adjusted into an SDS (12.5%) or native gel (6%). After electrophoresis, proteins were transferred to a nitrocellulose membrane (Amersham Biosciences Corp.). The blot was incubated with the HRP-conjugated goat anti-human Hb antibody (Cat. No. ab19362-1; Abcam Plc) at a dilution of 1:5000 for 2 h; with the mouse anti-human ferryl hemoglobin antibody (made by our groups) at a dilution of 1:1000 for 2 h. The antigen/antibody complex was detected with the chemiluminescence system according to the manufacturer's instructions (GE Healthcare Life Sciences). Quantification of the signals was performed using ImageJ software.

Analysis of various redox states of human Hb in human carotid arteries

Human healthy carotid arteries ($N=11$), atheromatous plaques ($N=11$), and complicated lesions ($N=11$) were homogenized under liquid nitrogen followed by the uptake of specimens with saline. Then, the samples were centrifuged (12,000 g, 15 min, 4°C) and the supernatants were measured with a spectrophotometer (Beckman Coulter, Inc.). The following equations were applied to measure the oxyHb, metHb, and ferrylHb contents of healthy carotid arteries, atheromatous plaques, and complicated lesions (44).

$$[OxyHb] = -75.78OD_{560} + 103.16OD_{576} - 38.39OD_{630}$$

$$[MetHb] = -26.09OD_{560} + 12.48OD_{576} - 280.70OD_{630}$$

$$[FerrylHb] = 132.6OD_{560} - 74.10OD_{576} - 68.33OD_{630}.$$

Separation of human blood-derived monocytes and treatment of macrophages

Human monocytes were collected from the blood of healthy donors. Phase centrifugation on Histopaque-1077 was used for monocyte separation. Cells were cultured in Dulbecco's modified Eagle's medium (DMEM) containing 15% FBS for 6 days in the presence of 50 ng/mL of M-CSF. After 6 days, macrophages were treated with 10 μM of heme, or 10 μM of Hb, or 10 μM of ferrylHb for 4, 8, 12, 16, 24, and 48 h at 37°C in 0% FBS containing DMEM.

Inhibition of actin polymerization

Macrophages grown on coverslips were treated with LAT A (500 nM; L5288-1MG) and LAT B (10 μM; L5163-100UG) and then exposed to ferrylHb (10 μM) for 16 h. Immunofluorescence staining was performed as described in the paragraph of immunofluorescent staining.

Analysis of PI3K/HIF-1α/VEGF pathway in macrophages

Human macrophages were exposed to 10 μM oxyHb or 10 μM ferrylHb for 2 h. In other experiments, human

macrophages were exposed to 10 μM heme, oxyHb, metHb, or ferrylHb for 16 h. The expression of PI3K ($n=3$), phopsho-PI3K ($n=3$), and HIF-1α ($n=5$) was assessed by Western blot. After treatment, the cells were solubilized in protein lysis buffer (in case of PI3K, HIF-1α proteins) or protein lysis buffer completed with phosphatase inhibitor (in case of phopsho-PI3K). Twenty micrograms of total protein was applied to 10% SDS-PAGE gels. Gels were blotted to the PVDF membrane and blocked with 5% BSA. Proteins were incubated with the following antibodies overnight: mouse anti-human PI3K antibody (MA1-74183; dilution: 1:500; Invitrogen), rabbit anti-human phospho-PI3K antibody (PA5-104853; dilution: 1:500; Invitrogen), rabbit anti-human HIF-1α antibody (PA1-16601; dilution: 1:500; Invitrogen) followed by HRP-conjugated mouse (ab6728; Abcam Plc) or rabbit secondary antibody (ab6721; Abcam Plc) at a dilution of 1:4000 for 2 h. Human macrophages were exposed to 10 μM heme, oxyHb, metHb, or ferrylHb for 24 h. The secreted level of VEGF-A was measured with the enzyme-linked immunosorbent assay (ELISA) kit according to the manufacturer's instructions (RAB0507; Sigma).

Immunofluorescent staining

Cells were fixed in 3.7% formaldehyde for 15 min and then permeabilized with 0.3% Triton X-100 for 15 min. F-actin was stained with iFluor 647-conjugated phalloidin at a 1:1000 dilution of the stock solution (Leica Microsystem, Mannheim, Germany) according to the manufacturer's instructions. Lysosomes were stained with Alexa Fluor 488 F(ab')2 fragment of goat anti-rabbit IgG (H+L, Cat. No. A11070; Thermo Fisher Scientific, Inc., Waltham, MA) secondary antibody-labeled anti-LAMP-1 (rabbit, Cat. No. ab24170; Abcam Plc) antibody (Leica Microsystem). FerrylHb is stained with Alexa Flour 568 F(ab')2 fragment of goat anti-mouse IgG (H+L, Cat. No. A11004; Thermo Fisher Scientific, Inc.) secondary antibody-labeled mouse monoclonal antibody and nuclei are stained with Hoechst 33258. LAMP-1 and ferrylHb antibodies were incubated at 1:500 dilution for 1 h at room temperature. All secondary antibodies were used at 1:500 dilution for 1 h at room temperature. In other cases, healthy arteries ($N=9$), atheroma plaques ($N=9$), hemorrhaged plaques ($N=9$), or macrophages were labeled with the mouse anti-human ferrylHb antibody (dilution of 1:1000 for 2 h) and stained with Alexa Flour 488 F(ab')2 fragment of goat anti-mouse IgG (H+L) at a dilution of 1:1000 for 2 h (Cat. No. A11070; Thermo Fisher Scientific, Inc.) or labeled with rabbit anti-human CD163 antibody (NB110-40686; Novusbio) at a dilution of 1:1000 for 2 h and stained with Alexa Flour 647 of goat anti-rabbit IgG (H+L) at a dilution of 1:1000 for 2 h (Cat. No. A21244; Thermo Fisher Scientific, Inc.). Second antibody control stainings for Figure 6 and Figure 12 were added as Supplementary Figures (Supplementary Figs. S6 and S7).

STED nanoscopy

Multicolor STED images were acquired with a Leica TCS SP8 using continuous-wave STED gated nanoscopy (Leica Microsystem). Gated STED images were deconvolved using Huygens Professional (Scientific Volume Imaging B.V., Hilversum, Netherlands) software.

CD163 gene silencing of macrophages

HiPerFect transfection reagent (3.0% vol/vol; Qiagen; 301705) was mixed with siRNA against CD163 (s17838; Ambion™) at a final concentration of 200 nM in a minimal serum content medium (Opti-MEM;31958-047; Lot. 1782606; Gibco) for a total reaction volume of 375 μL/sample. The incubation time of complex formation was 12 min at room temperature, and then, complexes were added to macrophages and placed into the incubator at 37°C for 6 h. After transfection time, the reactions were stopped by adding 15% FBS content DMEM, and at 72 h, macrophages were used for experiments.

Quantitative real-time polymerase chain reaction

Human macrophages were treated as indicated before. Total RNA was isolated using RNAzol STAT-60 according to the manufacturer's instructions (Tl-4120; Tel-Test, Inc., Friendswood, TX). RNA concentration was measured with the Implen N50 nanophotometer (Implen GmbH, München, Germany). After that, complementary DNA (cDNA) synthesis was performed using a high-capacity cDNA kit (43-688-13; Applied Biosystems, Foster City, CA). RT-qPCR technique was used for quantification of mRNA levels of *HO-1, IL-1β, TNF-α, CXCL8, CD163, CD209, IL-26RA*, glyceraldehyde 3-phosphate dehydrogenase (*GAPDH*), and *PPIA*. All primers were purchased from Thermo Fisher Scientific, Inc. TaqMan Universal PCR Master Mix was purchased from Applied Biosystems (Cat. No. 4269510). We performed TaqMan qPCR with a Bio-Rad CFX96 detection system (Bio-Rad Laboratories, Inc., Hercules, CA). Results were expressed as mRNA expression normalized to *GAPDH* or *PPIA*.

Production and labeling of monoclonal antibodies against ferrylHb

Balb/c mice (8 to 12 weeks old) were immunized subcutaneously with 100 μg ferrylHb emulsified incomplete Freund's adjuvant. Twenty micrograms of antigen adsorbed on the aluminum hydroxide gel was administered intraperitoneally as booster immunizations on two occasions in 2-week intervals. Four days before cell fusion, a final boost of 20 μg antigen was given intraperitoneally. Immune spleen cells were fused with Sp2/o myeloma cells according to the standard protocol. Hybridoma supernatants were tested for reaction with ferrylHb in indirect ELISA systems and Western blotting. The limiting dilution technique was used for cloning positive cultures. Antibodies were isolated from the culture medium using Protein G affinity chromatography. The selected ferrylHb monoclonal antibody (Isotype: IgG1) was labeled with HRPO using the method described by Wilson and Nakane (74).

Epitope mapping of the ferrylHb monoclonal antibody

The primary antibody (goat anti-mouse Fc-specific Ig) was bound to CNBr-Sepharose beads in compact reaction columns (CRC), and then the secondary antibody (monoclonal anti-ferrylHb antibody) was added and covalently cross-linked to the primary antibody. The washed and drained beads were incubated with 10 μg/mL ferrylHb in phosphate-buffered saline (PBS) or PBS alone at room temperature for

an hour. After washing with 0.1 *M* Tris/HCl (pH 8.5), 50 μL 1 μg/mL trypsin in 0.1 *M* Tris/HCl (pH 8.5) or 2 μg/mL Glu-C in phosphate buffer (pH 7.8) was added to the CRC and incubated overnight at 37°C. The supernatants were discarded and after washing the beads, peptides that remained bound to the antibody binding sites were analyzed in two different ways: (i) ∼1 μL of washed beads was mixed with 1 μL of CHCA matrix on the MALDI plate and air-dried (ii) and trypsin digested. The beads were analyzed by MALDI-TOF mass spectrometry on a Voyager DE STR (Applied Biosystems) operated in positive ion linear mode. The amino acid sequence of Hb subunit beta and Hb subunit alpha (Accession No. P68871 and P69905, respectively) was retrieved from the UniProt database and was subjected to *in silico* trypsin or Glu-C digestion by the PeptideCutter software. The m/z values from the acquired spectra were matched to peptides originating from the human Hb sequence.

In the case of tryptic digestion, peptides were eluted from the beads by 1% acetic acid and were subjected to LC-MS/MS-based analysis. Five microliters of sample was injected into the Easy nLC II (Bruker) nano high performance liquid chromatography. The separation of the peptides was done using a 90-min water/acetonitrile gradient on the Zorbax 300SB-C18 analytical column (150 mm × 75 μm, 3.5 μm particle size, 5 Å pore size; Agilent Technologies, Santa Clara, CA). Solvent A was 0.1% formic acid in LC water and solvent B was acetonitrile with 0.1% formic acid. The flow rate was 300 nL/min during the analyses. The eluted peptides were introduced into the 4000 QTRAP (ABSciex) mass spectrometer using a NanoSpray II MicroIon Source and controlled by the Analyst 1.4.2 software (ABSciex). The spray voltage was 2800 V, the ion source gas was 50 psi, the curtain gas was 20 psi, and the source temperature was 70°C. Information-dependent acquisition was applied selecting the two most intensive ions for fragmentation and acquisition of MS/MS spectra. The protein identification was made with ProteinPilot 4.5 (ABSciex) software and those peptides were accepted as identified where the confidence was higher than 90% and the series of b or y ions were present in the spectra.

SRM analysis

SRM transitions corresponding to the LLVVYPWTQR peptide were designed in Skyline (MacCoss Lab Software). All the possible transitions were included into the method file and after optimization, collision energy and declustering potential were used for the mass spectrometry analysis of tryptic peptides. The parameters for chromatographic separation and mass spectrometry were similar to those applied in the case of LC-MS/MS analyses, except that for LC separation, a 30-min gradient was used, and for the mass spectrometry analyses, the positive ion multiple reaction monitoring mode was selected. For data analysis, Skyline was used.

Molecular dynamic simulations

Starting from the X-ray structure deposited to the PDB protein data bank (PDB ID = 2dn2), molecular dynamics simulations were carried out on Hb α,β dimeric form to disclose the effect of the probable Y36 radical formation. For the protein, gromos53a6 force field was used. Since

there is no tyrosine radical parameter in this force field, it was introduced by deleting the proton from the tyrosine OH and keeping all the necessary parameters except the atomic partial charge parameters, which were reassigned replacing the phenolic Cξ-O-H (0.203, −0.611, 0.408, respectively) by 0.45 and −0.45 values for the Cξ-O atoms of the tyrosine radical. The model was then solvated in a dodecahedral box in a way that the distance between the box wall and the closest protein atom was at least 12 Å. The systems were neutralized and the ionic strength was set to 0.15 *M* by additional Na$^+$ and Cl$^-$ ions, the atomic positions were optimized (20,000 steps), and the system was heated up to 310 K during 2 ns. Then, 2 μs constant particle number (N), constant pressure (P = 105Pa), and constant temperature (T = 310 K) production dynamics with periodic boundary condition took place. To be able to apply a longer time step (4 fs) and this way to reach a longer total simulation time (2 μs), a virtual site protocol was used. For the solvent, simple point-charge explicit water model was applied. The long-range electrostatic energy corrections were calculated by means of the particle mesh Ewald (PME) method, while for the short-range electrostatic and van der Waals energy terms, 10 Å cutoff distances were used. For temperature coupling the v-rescale algorithm, and for pressure coupling the Berendsen method was used. The GROMACS software suites were used for all the simulations and for the analyses of the trajectories. Protein structure visualizations were done by the 1.9.2 version of the VMD software tools.

Examination of Hb oxidation with mass spectrometry

The LC-MS/MS analysis of trypsin digested samples was carried out on Easy nLC 1200 ultra performance liquid chromatography (UPLC) coupled to the Orbitrap Fusion mass spectrometer (Thermo Scientific, Waltham, MA) as described previously (30, 45). Briefly, following a 180-min-long chromatographic separation with water/acetonitrile gradient, the top 14 ions were selected for MS/MS analyses (Orbitrap analyzer resolution: 60,000, AGC target: 4.0e5). Collision-induced dissociation fragmentation was performed in the linear ion trap with 35% normalized collision energy (AGC target: 2.0e3). Dynamic exclusion for 45 s was enabled. Protein identification was done with MaxQuant 1.6.2.10 software (15) searching against the Human SwissProt database (release: 2020.02, 20,394 sequence entries). Cys oxidation, trioxidation, and carbamidomethylation along with Met oxidation and N-terminal acetylation were set as variable modifications. Maximum two missed cleavage sites were allowed. The results were imported into the Scaffold 4.8.9 software (Proteome Software, Inc.). Hb was visualized with CAVER Analyst 2.0 software using PDB entry 1BUW (35).

Immunoprecipitation of carotid artery samples

Healthy arteries (N = 3), atheroma plaques (N = 3), and hemorrhaged plaques (N = 3) were homogenized in liquid nitrogen. Then, the samples were solubilized in protein lysis buffer (10 m*M* Tris-HCl, 5 m*M* EDTA, and 150 m*M* NaCl (pH 7.2), 1% Triton X-100, 0.5% Nonidet P-40, and protease inhibitors (Complete Mini; F. Hoffmann-La Roche Ltd.). Pierce Protein A/G™ magnetic agarose beads (40 μL,

Cat. No. 78609; Thermo Scientific, Waltham, MA) were added to a 1.5 mL microcentrifuge tube. A total of 460 μL of binding/wash buffer (10 mM phosphate buffer [pH 7.4], 150 mM NaCl) was added to the beads. The tube was placed into a magnetic stand to collect the beads against the side of the tube. The supernatant was removed and discarded. Binding/wash buffer (0.5 mL) was added to the tube and gently mixed for 1 min. The beads were collected with the magnetic stand, and the supernatant was removed and discarded. The primary antibody at a 10-fold higher concentration than that used for Western blotting was added to a total volume of binding/wash buffer of 500 μL. The antibody-bead mixture was incubated for 4 h at 4°C by gentle mixing on a suitable shaker. The tube was placed into a magnetic stand to collect the beads against the side of the tube, and the supernatant was removed and discarded. Binding/wash buffer (0.5 mL) was added to the tube and gently mixed for 1 min. The washing step was repeated twice. Fifteen microliters of tissue lysate was added with 450 μL of binding/wash buffer to a 1.5 mL microcentrifuge tube. The lysate-bead/antibody conjugate mixture was incubated at 4°C under rotary agitation for 16 h. The beads were washed three times with binding/wash buffer containing a 1:20 volume of protease inhibitor. The tube was placed into a magnetic stand to collect the beads against the side of the tube, and the supernatant was removed and discarded. One hundred microliters of elution buffer (0.1 M glycine, pH 2.0–3.0) was added to the tube and incubated for 10 min at room temperature with occasional mixing. The beads were collected with a magnetic stand, and the supernatant was then removed and saved. To neutralize the low pH, 100 μL of neutralization buffer (1 M Tris-HCl, pH 7.5) was added for each 100 μL of eluate. Western blotting was used to assess ferrylHb in carotid artery samples.

Isolation and proteomic analysis of lysosomes

Lysosome Enrichment Kit for Tissue and Cultured Cells was used according to the manufacturer's guidance and instructions (89839; Thermo Fisher Scientific, Inc.). Macrophages were exposed to 10 μM of ferrylHb for 24 in 0% FBS containing DMEM. For protein analysis, lysosomes were solubilized in protein lysis buffer (10 mM Tris-HCl, 5 mM EDTA, 150 mM NaCl (pH 7.2), 1% Triton X-100, 0.5% Nonidet P-40, and protease inhibitors (Complete Mini; F. Hoffmann-La Roche Ltd.)). Then, 6 μg of protein of each sample was loaded on SDS-PAGE (10%). The blots were incubated with the mouse anti-human ferrylHb antibody (developed by our groups) at a dilution of 1:1000 or rabbit anti-human LAMP-1 (Cat. No. ab24170; Abcam Plc) antibody at a dilution of 1:500 or rabbit anti-human GAPDH at a dilution of 1:2500 for 16 h, followed by incubation with the HRP-conjugated secondary antibody for 2 h.

RNA-sequencing (NCBI SRA database under accession No. PRJNA594843)

To obtain global transcriptome data of ferrylHb-stimulated human macrophages, carotid artery samples from patients with atherosclerotic lesions type IV (atheromatous), type VI (complicated, intensively stained for ferrylHb), and healthy carotid arteries from cadavers of suicide or traumatic events, high-throughput mRNA se-

quencing analysis was performed on Illumina Sequencing Platform (Illumina, San Diego, CA). For this purpose, three sets of primary human macrophages were cultured in the presence of ferrylHb or vehicle for 8 h as described above. Total RNA was extracted and quantified, and RNA sample quality was checked on Agilent BioAnalyzer using the Eukaryotic Total RNA Nano Kit (Agilent Technologies) according to the manufacturer's protocol. Samples with RNA integrity number (RIN) value >8 were accepted for the library preparation process. RNA-seq libraries were prepared from total RNA (200 ng) using the NEBNext® Ultra II RNA Sample Preparation Kit for Illumina (New England BioLabs, Ipswich, MA) according to the manufacturer's protocol. Briefly, poly-A tailed RNAs were purified by oligodT-conjugated magnetic beads and fragmented at 94°C for 15 min. First-strand cDNA was generated by random priming reverse transcription, and a second-strand synthesis step was performed to generate double-stranded cDNA. After the repairing ends and adapter ligation steps, adapter-ligated fragments were amplified in enrichment PCR, and finally, sequencing libraries were generated. Sequencing runs were executed on Illumina NextSeq500 instrument (Illumina) using single-end 75 cycle sequencing. Aligned sequencing data have been deposited into the NCBI SRA database under accession number PRJNA594843.

Analysis of RNA-seq data

Raw sequencing data (fastq) were aligned to human reference genome version GRCh37 using HISAT2 algorithm, and BAM files were generated. Downstream analysis was performed using StrandNGS software. BAM files were imported into the software and DESeq1 algorithm was used for normalization. To identify DE genes between untreated and ferrylHb-stimulated conditions, or between atherosclerotic lesions and healthy biopsies, analysis of variance (ANOVA) with Tukey *post hoc* test was used. Heatmaps and dot plots were drawn using R packages pheatmap and ggplot2.

GO analysis

Lists of DE genes were analyzed using the Panther tool (www.geneontology.org) and the GO Enrichment Analysis function to create a GO. GOs with fold enrichment ≥2 and p value <0.05 were selected and results were presented according to their $-\log_{10} p$ value. Bar graph was drawn using R package ggplot2.

Statistics

Data were analyzed by GraphPad Prism 5.02 software (GraphPad Software, Inc., La Jolla, CA). Data are expressed as mean ± standard error of the mean. Differences in means were analyzed by Student's t-test or one-way ANOVA with Dunett post-test as appropriate. $p < 0.05$ was considered significant.

Authors' Contributions

Designing research studies: Z.H., L.P., A.P., G.V., L.N., G.B., and J.B. Conducting experiments: Z.H., L.P., A.P., É.K., S.P., É.C., G.K., Z.C., K.É.S., and I.K. Providing

Supplementary Material

References

1. Abraham NG and Drummond G. CD163-mediated hemoglobin-heme uptake activates macrophage HO-1, providing an antiinflammatory function. *Circ Res* 99: 911–914, 2006.

2. Aderem A and Underhill DM. Mechanisms of phagocytosis in macrophages. *Annu Rev Immunol* 17: 593–623, 1999.

3. Alayash AI. βCysteine 93 in human hemoglobin: a gateway to oxidative stability in health and disease. *Lab Invest* 101: 4–11, 2021.

4. Alayash AI, Patel RP, and Cashon RE. Redox reactions of hemoglobin and myoglobin: biological and toxicological implications. *Antioxid Redox Signal* 3: 313–327, 2001.

5. Ashburner M, Ball CA, Blake JA, Botstein D, Butler H, Cherry JM, Davis AP, Dolinski K, Dwight SS, Eppig JT, Harris MA, Hill DP, Issel-Tarver L, Kasarskis A, Lewis S, Matese JC, Richardson JE, Ringwald M, Rubin GM, and Sherlock G. Gene ontology: tool for the unification of biology. The Gene Ontology Consortium. *Nat Genet* 25: 25–29, 2000.

6. Ayer A, Zarjou A, Agarwal A, and Stocker R. Heme oxygenases in cardiovascular health and disease. *Physiol Rev* 96: 1449–1508, 2016.

7. Balla G, Jacob HS, Eaton JW, Belcher JD, and Vercellotti GM. Hemin: a possible physiological mediator of low density lipoprotein oxidation and endothelial injury. *Arterioscler Thromb* 11: 1700–1711, 1991.

8. Balla G, Vercellotti GM, Muller-Eberhard U, Eaton J, and Jacob HS. Exposure of endothelial cells to free heme potentiates damage mediated by granulocytes and toxic oxygen species. *Lab Invest* 64: 648–655, 1991.

9. Balla J, Jacob HS, Balla G, Nath K, Eaton JW, and Vercellotti GM. Endothelial-cell heme uptake from heme proteins: induction of sensitization and desensitization to oxidant damage. *Proc Natl Acad Sci U S A* 90: 9285–9289, 1993.

10. Barger AC, Beeuwkes R, 3rd, Lainey LL, and Silverman KJ. Hypothesis: vasa vasorum and neovascularization of human coronary arteries. A possible role in the pathophysiology of atherosclerosis. *N Engl J Med* 310: 175–177, 1984.

11. Beyer M, Mallmann MR, Xue J, Staratschek-Jox A, Vorholt D, Krebs W, Sommer D, Sander J, Mertens C, Nino-Castro A, Schmidt SV, and Schultze JL. High-resolution transcriptome of human macrophages. *PLoS One* 7: e45466, 2012.

12. Bolisetty S, Zarjou A, Hull TD, Traylor AM, Perianayagam A, Joseph R, Kamal AI, Arosio P, Soares MP, Jeney V, Balla J, George JF, and Agarwal A. Macrophage and epithelial cell H-ferritin expression regulates renal inflammation. *Kidney Int* 88: 95–108, 2015.

13. Bories G, Colin S, Vanhoutte J, Derudas B, Copin C, Fanchon M, Daoudi M, Belloy L, Haulon S, Zawadzki C, Jude B, Staels B, and Chinetti-Gbaguidi G. Liver X receptor activation stimulates iron export in human alternative macrophages. *Circ Res* 113: 1196–1205, 2013.

14. Boyle JJ, Harrington HA, Piper E, Elderfield K, Stark J, Landis RC, and Haskard DO. Coronary intraplaque hemorrhage evokes a novel atheroprotective macrophage phenotype. *Am J Pathol* 174: 1097–1108, 2009.

15. Cox J and Mann M. MaxQuant enables high peptide identification rates, individualized p.p.b.-range mass accuracies and proteome-wide protein quantification. *Nat Biotechnol* 26: 1367–1372, 2008.

16. Czimmerer Z, Varga T, Poliska S, Nemet I, Szanto A, and Nagy L. Identification of novel markers of alternative activation and potential endogenous PPARgamma ligand production mechanisms in human IL-4 stimulated differentiating macrophages. *Immunobiology* 217: 1301–1314, 2012.

17. Daemen MJ, Ferguson MS, Gijsen FJ, Hippe DS, Kooi ME, Demarco K, van der Wal AC, Yuan C, and Hatsukami TS. Carotid plaque fissure: an underestimated source of intraplaque hemorrhage. *Atherosclerosis* 254: 102–108, 2016.

18. Delbosc S, Bayles RG, Laschet J, Ollivier V, Ho-Tin-Noé B, Touat Z, Deschildre C, Morvan M, Louedec L, Gouya L, Guedj K, Nicoletti A, and Michel J-B. Erythrocyte efferocytosis by the arterial wall promotes oxidation in early-stage atheroma in humans. *Front Cardiovasc Med* 4: 43, 2017.

19. Deterding LJ, Ramirez DC, Dubin JR, Mason RP, and Tomer KB. Identification of free radicals on hemoglobin from its self-peroxidation using mass spectrometry and immuno-spin trapping: observation of a histidinyl radical. *J Biol Chem* 279: 11600–11607, 2004.

20. Etzerodt A, Maniecki MB, Møller K, Møller HJ, and Moestrup SK. Tumor necrosis factor α-converting enzyme (TACE/ADAM17) mediates ectodomain shedding of the scavenger receptor CD163. *J Leukoc Biol* 88: 1201–1205, 2010.

21. Finn AV, Nakano M, Polavarapu R, Karmali V, Saeed O, Zhao XQ, Yazdani S, Otsuka F, Davis T, Habib A, Narula J, Kolodgie FD, and Virmani R. Hemoglobin directs macrophage differentiation and prevents foam cell formation in human atherosclerotic plaques. *J Am Coll Cardiol* 59: 166–177, 2012.

22. Gerrick KY, Gerrick ER, Gupta A, Wheelan SJ, Yegnasubramanian S, and Jaffee EM. Transcriptional profiling identifies novel regulators of macrophage polarization. *PLoS One* 13: e0208602, 2018.

23. Graversen JH, Madsen M, and Moestrup SK. CD163: a signal receptor scavenging haptoglobin-hemoglobin complexes from plasma. *Int J Biochem Cell Biol* 34: 309–314, 2002.

24. Gregory CD and Devitt A. The macrophage and the apoptotic cell: an innate immune interaction viewed simplistically? *Immunology* 113: 1–14, 2004.

25. Guo L, Akahori H, Harari E, Smith SL, Polavarapu R, Karmali V, Otsuka F, Gannon RL, Braumann RE, Dickinson MH, Gupta A, Jenkins AL, Lipinski MJ, Kim J, Chhour P, de Vries PS, Jinnouchi H, Kutys R, Mori H, Kutyna MD, Torii S, Sakamoto A, Choi CU, Cheng Q, Grove ML, Sawan MA, Zhang Y, Cao Y, Kolodgie FD, Cormode DP, Arking DE, Boerwinkle E, Morrison AC, Erdmann J, Sotoodehnia N, Virmani R, and Finn AV. CD163$^+$ macrophages promote angiogenesis and vascular permeability accompanied by inflammation in atherosclerosis. *J Clin Invest* 128: 1106–1124, 2018.

26. Gutiérrez-Muñoz C, Méndez-Barbero N, Svendsen P, Sastre C, Fernández-Laso V, Quesada P, Egido J, Escolá-Gil JC, Martín-Ventura JL, Moestrup SK, and Blanco-Colio LM. CD163 deficiency increases foam cell formation and plaque progression in atherosclerotic mice. *FASEB J* 34: 14960–14976, 2020.

27. Harel S and Kanner J. The generation of ferryl or hydroxyl radicals during interaction of haemproteins with hydrogen peroxide. *Free Radic Res Commun* 5: 21–33, 1988.

28. Harel S, Salan MA, and Kanner J. Iron release from metmyoglobin, methaemoglobin and cytochrome c by a system generating hydrogen peroxide. *Free Radic Res Commun* 5: 11–19, 1988.

29. Hawkins PT and Stephens LR. PI3K signalling in inflammation. *Biochim Biophys Acta Mol Cell Biol Lipids* 1851: 882–897, 2015.

30. Jana S, Strader MB, and Alayash AI. The providence mutation (βK82D) in human hemoglobin substantially reduces βCysteine 93 oxidation and oxidative stress in endothelial cells. *Int J Mol Sci* 21: 9453, 2020.

31. This reference has been deleted.

32. Jeney V, Balla J, Yachie A, Varga Z, Vercellotti GM, Eaton JW, and Balla G. Pro-oxidant and cytotoxic effects of circulating heme. *Blood* 100: 879–887, 2002.

33. Jia Y, Buehler PW, Boykins RA, Venable RM, and Alayash AI. Structural basis of peroxide-mediated changes in human hemoglobin: a novel oxidative pathway. *J Biol Chem* 282: 4894–4907, 2007.

34. Johnson JL and Newby AC. Macrophage heterogeneity in atherosclerotic plaques. *Curr Opin Lipidol* 20: 370–378, 2009.

35. Jurcik A, Bednar D, Byska J, Marques SM, Furmanova K, Daniel L, Kokkonen P, Brezovsky J, Strnad O, Stourac J, Pavelka A, Manak M, Damborsky J, and Kozlikova B. CAVER Analyst 2.0: analysis and visualization of channels and tunnels in protein structures and molecular dynamics trajectories. *Bioinformatics* 34: 3586–3588, 2018.

36. Kassa T, Jana S, Meng F, and Alayash AI. Differential heme release from various hemoglobin redox states and the upregulation of cellular heme oxygenase-1. *FEBS Open Bio* 6: 876–884, 2016.

37. Kristiansen M, Graversen JH, Jacobsen C, Sonne O, Hoffman HJ, Law SK, and Moestrup SK. Identification of the haemoglobin scavenger receptor. *Nature* 409: 198–201, 2001.

38. Lamaze C, Fujimoto LM, Yin HL, and Schmid SL. The actin cytoskeleton is required for receptor-mediated endocytosis in mammalian cells. *J Biol Chem* 272: 20332–20335, 1997.

39. Lardinois OM, Detweiler CD, Tomer KB, Mason RP, and Deterding LJ. Identifying the site of spin-trapping in proteins by a combination of liquid chromatography, ELISA and off-line tandem mass spectrometry. *Free Radic Biol Med* 44: 893–906, 2008.

40. Li W, Ostblom M, Xu L-H, Hellsten A, Leanderson P, Liedberg B, Brunk UT, Eaton JW, and Yuan X-M. Cytocidal effects of atheromatous plaque components: the death zone revisited. *FASEB J* 20: 2281–2290, 2006.

41. This reference has been deleted.

42. Libby P. Inflammation in atherosclerosis. *Nature* 420: 868–874, 2002.

43. Libby P, Ridker PM, and Maseri A. Inflammation and atherosclerosis. *Circulation* 105: 1135, 2002.

44. Meng F and Alayash AI. Determination of extinction coefficients of human hemoglobin in various redox states. *Anal Biochem* 521: 11–19, 2017.

45. Michael Brad S, Hicks WA, Kassa T, Singleton E, Soman J, Olson JS, Weiss MJ, Mollan TL, Wilson MT, and Alayash AI. Post-translational transformation of methionine to aspartate is catalyzed by heme iron and driven by peroxide: a novel subunit-specific mechanism in hemoglobin. *J Biol Chem* 289: 22342–22357, 2014.

46. Michel J-B, Martin-Ventura JL, Nicoletti A, and Ho-Tin-Noé B. Pathology of human plaque vulnerability: mechanisms and consequences of intraplaque haemorrhages. *Atherosclerosis* 234: 311–319, 2014.

47. Moore KJ and Tabas I. The cellular biology of macrophages in atherosclerosis. *Cell* 145: 341–355, 2011.

48. Moreno PR. Vulnerable plaque: definition, diagnosis, and treatment. *Cardiol Clin* 28: 1–30, 2010.

49. Moreno PR, Purushothaman K-R, Sirol M, Levy AP, and Fuster V. Neovascularization in human atherosclerosis. *Circulation* 113: 2245–2252, 2006.

50. Mosser DM and Edwards JP. Exploring the full spectrum of macrophage activation. *Nat Rev Immunol* 8: 958–969, 2008.

51. Nagy E, Eaton JW, Jeney V, Soares MP, Varga Z, Galajda Z, Szentmiklósi J, Méhes G, Csonka T, Smith A, Vercellotti GM, Balla G, and Balla J. Red cells, hemoglobin, heme, iron, and atherogenesis. *Arterioscler Thromb Vasc Biol* 30: 1347–1353, 2010.

52. Palazon A, Goldrath AW, Nizet V, and Johnson RS. HIF transcription factors, inflammation, and immunity. *Immunity* 41: 518–528, 2014.

53. Patel RP, Svistunenko DA, Darley-Usmar VM, Symons MC, and Wilson MT. Redox cycling of human methaemoglobin by H_2O_2 yields persistent ferryl iron and protein based radicals. *Free Radic Res* 25: 117–123, 1996.

54. Pimenova T, Pereira CP, Gehrig P, Buehler PW, Schaer DJ, and Zenobi R. Quantitative mass spectrometry defines an oxidative hotspot in hemoglobin that is specifically protected by haptoglobin. *J Proteome Res* 9: 4061–4070, 2010.

55. Potor L, Bányai E, Becs G, Soares MP, Balla G, Balla J, and Jeney V. Atherogenesis may involve the prooxidant and proinflammatory effects of ferryl hemoglobin. *Oxid Med Cell Longev* 2013: 676425, 2013.

56. Ramirez DC, Chen YR, and Mason RP. Immunochemical detection of hemoglobin-derived radicals formed by reaction with hydrogen peroxide: involvement of a protein-tyrosyl radical. *Free Radic Biol Med* 34: 830–839, 2003.

57. Reeder BJ, Cutruzzola F, Bigotti MG, Hider RC, and Wilson MT. Tyrosine as a redox-active center in electron transfer to ferryl heme in globins. *Free Radic Biol Med* 44: 274–283, 2008.

58. Reeder BJ, Grey M, Silaghi-Dumitrescu R-L, Svistunenko DA, Bülow L, Cooper CE, and Wilson MT. Tyrosine residues as redox cofactors in human hemoglobin: implications for engineering nontoxic blood substitutes. *J Biol Chem* 283: 30780–30787, 2008.

59. Ross R. Atherosclerosis—an inflammatory disease. *N Engl J Med* 340: 115–126, 1999.

60. Rouault TA. The role of iron regulatory proteins in mammalian iron homeostasis and disease. *Nat Chem Biol* 2: 406–414, 2006.

61. Schaer CA, Schoedon G, Imhof A, Kurrer MO, and Schaer DJ. Constitutive endocytosis of CD163 mediates hemoglobin-heme uptake and determines the noninflammatory and protective transcriptional response of macrophages to hemoglobin. *Circ Res* 99: 943–950, 2006.

62. Schaer DJ, Schaer CA, Buehler PW, Boykins RA, Schoedon G, Alayash AI, and Schaffner A. CD163 is the macrophage scavenger receptor for native and chemically modified hemoglobins in the absence of haptoglobin. *Blood* 107: 373–380, 2006.

63. Schrijvers DM, De Meyer GRY, Kockx MM, Herman AG, and Martinet W. Phagocytosis of apoptotic cells by macrophages is impaired in atherosclerosis. *Arterioscler Thromb Vasc Biol* 25: 1256–1261, 2005.

64. Shaik-Dasthagirisaheb YB, Varvara G, Murmura G, Saggini A, Potalivo G, Caraffa A, Antinolfi P, Tete' S, Tripodi D, Conti F, Cianchetti E, Toniato E, Rosati M, Conti P, Speranza L, Pantalone A, Saggini R, Theoharides TC, and Pandolfi F. Vascular endothelial growth factor (VEGF), mast cells and inflammation. *Int J Immunopathol Pharmacol* 26: 327–335, 2013.

65. Siems WG, Sommerburg O, and Grune T. Erythrocyte free radical and energy metabolism. *Clin Nephrol* 53: S9–S17, 2000.

66. Sikura KÉ, Potor L, Szerafin T, Zarjou A, Agarwal A, Arosio P, Poli M, Hendrik Z, Méhes G, Oros M, Posta N, Beke L, Fürtös I, Balla G, and Balla J. Potential role of H-ferritin in mitigating valvular mineralization. *Arterioscler Thromb Vasc Biol* 39: 413–431, 2019.

67. Silva G, Jeney V, Chora A, Larsen R, Balla J, and Soares MP. Oxidized hemoglobin is an endogenous proinflammatory agonist that targets vascular endothelial cells. *J Biol Chem* 284: 29582–29595, 2009.

68. Soares MP and Hamza I. Macrophages and iron metabolism. *Immunity* 44: 492–504, 2016.

69. Stary HC, Chandler AB, Dinsmore RE, Fuster V, Glagov S, Insull W, Jr., Rosenfeld ME, Schwartz CJ, Wagner WD, and Wissler RW. A definition of advanced types of atherosclerotic lesions and a histological classification of atherosclerosis. A report from the Committee on Vascular Lesions of the Council on Arteriosclerosis, American Heart Association. *Circulation* 92: 1355–1374, 1995.

70. The Gene Ontology Consortium. The Gene Ontology Resource: 20 years and still GOing strong. *Nucleic Acids Res* 47: D330–D338, 2018.

71. Torti SV, Kwak EL, Miller SC, Miller LL, Ringold GM, Myambo KB, Young AP, and Torti FM. The molecular cloning and characterization of murine ferritin heavy chain, a tumor necrosis factor-inducible gene. *J Biol Chem* 263: 12638–12644, 1988.

72. Van Gorp H, Delputte PL, and Nauwynck HJ. Scavenger receptor CD163, a Jack-of-all-trades and potential target for cell-directed therapy. *Mol Immunol* 47: 1650–1660, 2010.

73. Weaver LK, Pioli PA, Wardwell K, Vogel SN, and Guyre PM. Up-regulation of human monocyte CD163 upon activation of cell-surface Toll-like receptors. *J Leukoc Biol* 81: 663–671, 2007.

74. Wilson MB and Nakane PK. Recent development in the periodate method of conjugating horseradish peroxidase (HRPO) to antibodies. In: *Immunofluorescence and Related Staining Techniques.* Elsevier/North-Holland Biomed. Press, Amsterdam, New York: Elsevier, 1978, pp. 215–224.

75. Winterbourn CC. Oxidative reactions of hemoglobin. *Methods Enzymol* 186: 265–272, 1990.

76. Yuan XM, Anders WL, Olsson AG, and Brunk UT. Iron in human atheroma and LDL oxidation by macrophages following erythrophagocytosis. *Atherosclerosis* 124: 61–73, 1996.

77. Yuan XM, Brunk UT, and Olsson AG. Effects of iron- and hemoglobin-loaded human monocyte–derived macrophages on oxidation and uptake of LDL. *Arterioscler Thromb Vasc Biol* 15: 1345–1351, 1995.

78. Yuan XM, Olsson AG, and Brunk UT. Macrophage erythrophagocytosis and iron exocytosis. *Redox Rep* 2: 9–17, 1996.

Address correspondence to:
Prof. József Balla
Division of Nephrology
Department of Medicine
Faculty of Medicine
University of Debrecen
Nagyerdei krt. 98., Pf. 19
4032 Debrecen
Hungary

E-mail: balla@belklinika.com

Abbreviations Used

2D = two dimensional
3D = three dimensional
ANOVA = analysis of variance
cDNA = complementary DNA
CRC = compact reaction columns
CW = continous wavelength
DE = differentially expressed
DMEM = Dulbecco's modified Eagle's medium
EC = endothelial cell
ELISA = enzyme-linked immunosorbent assay
FBS = fetal bovine serum
FC = fold change
GAPDH = glyceraldehyde 3-phosphate dehydrogenase
GO = Gene Ontology
H_2O_2 = hydrogen peroxide
Hb = hemoglobin

HIF-1α = hypoxia-inducible factor 1-alpha
HO-1 = heme oxygenase-1
ICAM-1 = intercellular adhesion molecule-1
LAMP-1 = lysosomal-associated membrane protein 1
LAT A = latrunculin A
LAT B = latrunculin B
LDL = low-density lipoprotein
LOOH = lipid hydroperoxides
mRNA = messenger RNA
ns = not significant
oxLDL = oxidized low-density lipoprotein
oxPL = oxidized plaque lipid
PBS = phosphate-buffered saline
PI3K = phosphoinositide 3-kinase
RBC = red blood cell
RT-qPCR = real-time quantitative polymerase chain reaction
SD = standard deviation
siRNA = small interfering RNA
STED = stimulated emission depletion
VCAM-1 = vascular cell adhesion molecule-1
VEGF = vascular endothelial growth factor